

**Determination of Impurity
Concentrations and Z_{eff} by
VUV Spectroscopy on ASDEX**

G. Janeschitz, L.B. Ran*, G. Fussmann,
K. Krieger, K.-H. Steuer, and the ASDEX Team

IPP III/147

November 1990



MAX-PLANCK-INSTITUT FÜR PLASMAPHYSIK

8046 GARCHING BEI MÜNCHEN

MAX-PLANCK-INSTITUT FÜR PLASMAPHYSIK
GARCHING BEI MÜNCHEN

**Determination of Impurity
Concentrations and Z_{eff} by
VUV Spectroscopy on ASDEX**

G. Janeschitz, L.B. Ran*, G. Fussmann,
K. Krieger, K.-H. Steuer, and the ASDEX Team

IPP III/147

November 1990

*Die nachstehende Arbeit wurde im Rahmen des Vertrages zwischen dem
Max-Planck-Institut für Plasmaphysik und der Europäischen Atomgemeinschaft über
die Zusammenarbeit auf dem Gebiete der Plasmaphysik durchgeführt.*

**Determination of Impurity
Concentrations and Z_{eff} by
VUV Spectroscopy on ASDEX**

G. Janeschitz, L. B. Ran*, G. Fussmann,
K. Krieger, K. H. Steuer, and the ASDEX team

IPP III/147

Nov. 1989

Abstract: The impurity concentrations and corresponding Z_{eff} contributions as well as the dilution of the deuterium background plasma in ASDEX are determined by VUV spectroscopy. The methods used are described in detail. We describe the absolute calibration of our VUV survey spectrometer with two different calibration sources, as well as our ZEDIFF time-dependent transport code, used for interpreting the spectroscopic measurements. The assessed spectroscopic Z_{eff} compares quite well with the bremsstrahlung Z_{eff} as demonstrated for a number of representative ohmically and additionally heated discharges.

In order to obtain these results readily on a shot-to-shot basis at the end of each discharge, a simplified fast evaluation method is introduced. This fast analysis method yields the central impurity concentrations, the central Z_{eff} contributions, and the dilution of the deuterons. Again, the results from the fast analysis method agree well with those from our extended transport code treatment and with the bremsstrahlung Z_{eff} .

* Permanent address: Southwestern Institute of Physics, Leshan, P.R. of China

1. Introduction

A knowledge of the impurity concentrations in a tokamak discharge is very important for determining the quality of the plasma, especially during auxiliary heating (NBI, ICRH). Whereas only final results are generally reported, this paper also reviews the methods used and the uncertainties inherent in obtaining absolute impurity densities from spectroscopic measurements. To this end we describe in some detail our ZEDIFF impurity transport code (section 3), which is an indispensable tool for interpreting such measurements.

In contrast to similar codes, ZEDIFF is also capable of treating strongly time-dependent events, this property being necessary for simulating many of the impurity phenomena observed on ASDEX.

As the input data required for this code are complex and call for time-consuming calculations on the Cray computer, it cannot be used for standard shot-to-shot evaluation. It was therefore necessary to develop a simplified fast version, which was done analogously to a procedure suggested by Behringer [1]. This fast analysis method based on a two-dimensional parameterisation using ZEDIFF code results, is described in section 5.

Another crucial point in obtaining impurity densities is the calibration of the instruments. The methods used to calibrate our VUV survey spectrometer (of SPRED type, [3]) are reported in section 2.

We exemplify the different evaluation methods by referring to some density sequences of ASDEX discharges with and without auxiliary heating. The contributions of light and metallic impurities to Z_{eff} and the effect of the deuterium dilution are documented for various heating conditions. We also compare the spectroscopically determined Z_{eff} with independent measurements of infrared bremsstrahlung.

* Permanent address: Southwestern Institute of Physics, Leshan, P.R. of China

2. Absolutely measured line intensities

Determining absolute impurity densities first requires, absolute measurement of representative line intensities. These can be measured with the ASDEX VUV SPRED spectrometer, which monitors the wavelength range from 10 nm to 110 nm with a time resolution of 26.7 ms (Fig. 1). Needless to say, calibration of instruments in this wavelength range is rather complicated even when synchrotron radiation is used [3]. We decided to calibrate the SPRED spectrometer with two different light sources each of which radiates several absolute line intensities. Together they cover the whole wavelength range of the spectrometer.

The first light source, developed at the University of Giessen [4], consists mainly of an electron beam passing through a gas volume; the beam current and the gas pressure are absolutely measured. The line intensities are then calculated by using well known excitation rate coefficients [5]. This source was used to calibrate a McPherson one-metre normal-incidence spectrometer in the wavelength range from 45 nm to 120 nm. The absolute sensitivity of the SPRED over the upper half of its spectral range was obtained by comparing the intensities of several impurity lines measured with both spectrometers during the same ASDEX discharge (Fig. 2).

The wavelength range below 58.4 nm was covered by a hollow cathode source developed by the University of Hannover [6]. This particular source was calibrated by BTB Berlin by means of synchrotron radiation. It radiates several very intense lines (Al IV: 13.1, 16.0, 16.2 nm; He II: 24.3, 25.6, 30.4 nm; He I: 58.4 nm) and allows calibration with the same integration time (26.7 ms) used in recording ASDEX shots (peak count rate as high as $8.3 \times 10^5 \text{ s}^{-1}$ are obtained for the strongest lines). The combined calibration points cover the whole wavelength range of the SPRED spectrometer, as displayed in Fig. 2. This calibration curve already includes the solid angle of the instrument as used on ASDEX. The measured signals can thus be directly compared

with the results obtained from our ZEDIFF transport code. The accuracy of this calibration is estimated at approximately 20%.

3. ZEDIFF impurity transport code

The ZEDIFF impurity transport code, used to evaluate our spectroscopic measurements, was developed at ASDEX in 1984 and has been steadily extended and improved since then. It is based on Behringer's STRAHL code [7], which calculates the evolution of impurity densities from a given influx and known electron density and temperature profiles. STRAHL, however, was insufficient for simulating strongly heated (4 MW NI, 3 MW ICRH) high-confinement plasmas with their large electron density and temperature excursions accompanied by rapid changes of the ionisation equilibrium. Especially troublesome were discharges exhibiting transitions into the quiescent H-mode, or pellet-refuelled discharges, where the electron density and temperature do not reach steady-state conditions and the confinement properties of the plasma vary substantially. In the new code version, ZEDIFF, not only are the transport coefficients time-dependent, but also the n_e and T_e profiles of the background plasma. These electron density and temperature profiles are obtained from the ASDEX Thomson scattering diagnostic [8] every 17 ms during a discharge (Fig. 3). In the code, they are described by a time-dependent exponential fit function:

$$n_e(r,t) = 10^{14} \exp (a_{0n} + a_{1n} r^2 + a_{2n} r^4 + a_{3n} r^6),$$

$$T_e(r,t) = \exp (a_{0T} + a_{1T} r^2 + a_{2T} r^4 + a_{3T} r^6)$$

where the coefficients a_{in} and a_{iT} are all functions of time.

In order to get a smooth transition between two time points, the fit parameters and other time-dependent input parameters described below are linearly interpolated between these 17 ms time steps.

In order to control this rather complicated transport calculation a large number of time-dependent input parameters

and control flags have to be passed to the program. This is done by submitting to the Cray an input data file generated by the ZEDATA loading code. Besides writing the fit parameters of the electron density and temperature into the data file, ZEDATA also inserts the default values of all other input parameters and control flags, thus setting up the complete calculation structure. Important input parameters are the neutral impurity influxes together with the plasma edge parameters (n_e , T_e for $r > a$). Also important are the transport coefficients (D , V_{in}) for the core region of the plasma. These transport parameters can be changed time-dependently (in steps of 17 ms) during the calculation by changing the input data file. The following options are possible:

1. Anomalous transport with a radially constant diffusion coefficient ($D(r) = \text{const}$) and an inward drift velocity v_{in} having a linear or quadratic dependence on r (typical values: $D = 5000 \text{ cm}^2 \text{ s}^{-1}$ for C and O and $D = 4000 \text{ cm}^2 \text{ s}^{-1}$ for Fe, Cu in OH heating, $D = 9000 \text{ cm}^2 \text{ s}^{-1}$ in the L-mode of NI heating, $v_{in}(a) = 230 \text{ cm s}^{-1}$).

2. Neoclassical transport, with both the Pfirsch-Schlüter and the banana plateau regimes taken into account. [9]

3. A combination of anomalous and neoclassical transport. Furthermore, a number of other input-parameters are time-dependent and have to be defined in the input data file, e.g.

- recycling coefficients (divertor, wall);
- sawtooth induced transport in the central plasma region, (which is described by a short (1 ms) outward pulse around the $q=1$ surface);
- Elm-induced transport in the plasma edge region (the special ELM-features of the code as described below have to be defined).

A more detailed description of the input data file is listed in Appendix A.

Another important quantity with a major influence on the ionization equilibrium is the density profile of fast neutrals produced in the core of the plasma by neutral beam injection. To take these changes into account the neutral density profiles are calculated with the ZENEUT code by means of the measured

electron density, the temperature and the beam power, as well as the known species mix of the beams. The calculated profiles of four different energies (full (55 keV), 1/2, 1/3 and thermal) are fitted, again by using an exponential fit function similar to that for the electron density and temperature. The fit parameters obtained are then written into the input data file. A critical point of any quantitative impurity transport simulation is the description of the electron density and temperature profiles at the plasma boundary and especially in the scrape-off layer. In conjunction with the inward velocity of the neutral impurity atoms (V_0) they define the ionisation length and thus the source term. Together with the parallel and perpendicular transport in the scrape-off region, this source term defines the impurity screening efficiency of the scrape-off plasma. At ASDEX there is a special Thomson edge diagnostic for the electron temperature and density [10] which yields rather accurate data for the plasma boundary. This allows us to obtain a quantitative description of the screening of the scrape-off plasma [15] for the majority of the different ASDEX discharges. A second data file contains all the atomic data required to calculate the rates of ionisation, recombination, and excitation of prominent lines. The total radiation losses for each impurity species can also be obtained (Appendix B). After submitting the code and the two input data files to the Cray computer, the following quantities are calculated, plotted and stored in two data files for further processing: -

- time-dependent impurity density profile (or the impurity concentration profile (Fig. 4));
- particle balance (impurity influx, divertor and wall losses);
- time-dependent spatial distribution of line radiation (most prominent lines in the VUV or X-ray range) of four selected ionisation stages;
- line integrals along pre-selected lines of sight for the corresponding spectral lines for ready comparison with the experimental intensity signals;
- charge profile of the impurity ions (Fig. 5);

- total radiation profiles for comparison with bolometer measurements[9]; soft X-ray profiles (calculated from total radiation by applying the appropriate energy-dependent filter function);
- line integrals for the soft X-rays and total radiation (again for simple comparison with experimental time traces);
- central impurity density, soft-rays and total radiation; global particle confinement time for the impurities $\tau_z = N_z/\Phi_z$; total impurity content of the chosen element in the region of closed magnetic surfaces.

For special investigations some additional features can be activated:

To assess the divertor retention of gaseous impurities [10], the code is equipped with a simple divertor model that adds an additional neutral impurity flux Φ_D from the divertor:

$$\Phi_D = \frac{N_D}{\tau_D},$$

where τ_D is the particle confinement time for gaseous impurities in the divertor chamber. The number of particles N_D accumulated in the divertor is calculated from the equation

$$N_D = e^{-t/\tau_D} \int_0^t e^{t'/\tau_D} \Phi_{out}^+ dt',$$

where Φ_{out}^+ is the net flux of impurity ions leaving the scrape-off plasma and entering the divertor (mentioned above as divertor losses).

The ZEDIFF code also offers the possibility of studying time-dependent events including short gas puffs or oscillating gas puffing, laser blow-off, or sudden changes in transport, such as occur during an H-transition. These time-dependent phenomena can reasonably be used to determine the appropriate transport parameters for different confinement regimes.

Experience has been gained with this code during the last four years by comparing the simulations with measurements obtained

from various diagnostics (spectroscopy, bolometer, soft-rays, Z_{eff}) for different transport and heating scenarios (OH, NI-L, NI-H, ICRH, pellet, etc.). In general, the code results fit rather well with absolute line intensities measured by our VUV SPRED spectrometer and the global measurements of soft X-rays, total radiation and Z_{eff} . There is, however, a systematic deviation between the calculated total radiation and that measured (calc.rad*1.7 = measured rad.). This deviation can possibly be explained by an oversimplified treatment of the total radiated power (see the STRAHL report [7]).

4. Absolute impurity densities and Z_{eff}

As described in the previous section, the ZEDIFF code calculates the time-dependent radiation profiles, as well as the line integrals (dimension W/cm²) for the most prominent lines of up to four chosen ionisation stages for a given impurity species. As an example we present in Fig. 6 such calculated radiation profiles for the most prominent Cu XIX, Fe XVI, O VI and C IV lines for a combined beam and ICRF-heated L-mode discharge. In this discharge three time intervals can be distinguished: during the first period (0.8 - 1.7 s) 1MW of H⁰ beams and 2.0 MW of ICRH was applied, in the second period (1.7 - 2.0 sec) only 2.0 MW of ICRH was launched, while in the third period the plasma was heated by a combination of 1.2 MW of D⁰-beam injection and 2.0 MW of ICRH. The neutral impurity influx was adjusted in the calculation in such a way that the resulting central impurity density was approximately 10¹⁰ ions/cm³. This value is initially chosen arbitrarily. In order to determine the real impurity density, we compare the calculated line intensities (ZEDIFF) with those absolutely measured (SPRED):

$$n_z(r) = \frac{I_{\text{SPRED}}^z}{I_{\text{ZEDIFF}}^z} n_z^{\text{ZEDIFF}}(r) [\text{cm}^{-3}].$$

Dividing the total impurity density profiles by the electron density profile yields the impurity concentration profiles $\sum n_z(r)/n_e(r)$ shown in Fig. 4.

The highest central concentrations are found during the combined ICRH(2 MW) and D⁰-beam heating (1.2 MW) phase: Cu: 0.1%, Fe: 0.15%, O:1.0%, C: 2.5%. As is to be seen from Fig. 4, the concentration profiles are always hollow irrespective of the heating scenario or confinement regime (OH-mode, L-mode). This can be explained by the screening properties of the scrape-off layer, which retains approximately 90% of the impurity influx originating at the main chamber wall. Approximately 60 to 70% of the influx is transported directly into the divertor, which is described in the code by an average residence time τ for the particles in the scrape-off layer. The hollowness of the impurity concentration profiles can be slightly influenced by changing this residence time. In the case discussed here this time is set to 1 ms, corresponding approximately to 1/10 of the ion sound speed for the background ions on their way into the divertor.

If the calculated charge profile for all impurity species (Fig. 5), are taken into account, their contributions to the total $Z_{\text{eff}}(r,t)$ (Fig. 7a) and the dilution of the deuterons $Dil(r,t)$ (Fig.7b) are calculated according to

$$Z_{\text{eff}}(r) = \sum_{I=1}^{I_{\text{max}}} \frac{n_I(r)}{n_e(r)} Z_I^2,$$

$$Dil(r,t) = \frac{n_1}{n_e} = 1 - \sum_{I=2}^{I_{\text{max}}} \frac{n_I(r)}{n_e(r)} Z_I,$$

where $n_I(r)$ are the ion densities. The proton or deuteron densities with $Z_I=1$ are noted as n_1 . The corresponding charge profiles $Z(r) = \sum n_I(r) Z_I / \sum n_I(r)$ for each of the four elements are displayed in Fig. 5 .

The overall agreement between the Z_{eff} profiles obtained from VUV spectroscopy and the Z_{eff} profiles from bremsstrahlung [12] as displayed in Fig. 8, is rather satisfactory.

In Fig. 9 the time-dependent contributions of Cu, Fe, O, C to the central Z_{eff} are plotted for the same discharge. The resulting total Z_{eff} is compared with that obtained by the bremsstrahlung diagnostics (solid dots), good agreement again

being demonstrated. In Fig. 10 the profiles of the Z_{eff} contributions are plotted for three different time points during the discharge under three different heating conditions: during the first heating period (0.8 - 1.7 s), with $H^0 + \text{ICRH}$ Z_{eff} reaches nearly 3 in the centre (Figs. 9,10) and rises to 3.5 at the separatrix. Since no quantitative measurements of either bremsstrahlung or impurity concentrations exist in the scrape-off region, Z_{eff} is taken as constant outside the separatrix. The dilution of the deuterium background plasma is found to be already 20% in the plasma centre, rising to 50% at the separatrix. While the dilution is almost solely caused by the light impurities (O, C), the contribution to Z_{eff} from the two metallic impurities (Cu, Fe) is found to be already 30% of the total Z_{eff} . This difference can be understood from the different Z weighting in the above formulae. It should be pointed out that the hollowness of the total Z_{eff} profiles in all three cases shown in Fig. 10 is determined by the light impurities. While, however, the concentration profiles (Fig. 4) of all four impurities (Cu, Fe, O, C) are hollow, the charge profiles of the metallic impurities are peaked in contrast to those of oxygen and carbon (Fig. 5). Thus the very broad charge profiles of O and C together with the hollow concentration profiles are responsible for the hollowness of the Z_{eff} profiles. This hollowness is also confirmed by the bremsstrahlung profile measurements (Fig. 8).

During the second interval (1.7 - 2.0 s) with ICRF heating, the central Z_{eff} is reduced to 2.2 mainly by the reduction of Cu and Fe. This may be explained by the vanishing charge exchange sputtering from high energy neutrals in the main chamber (Fe), as well as by the strong reduction of the hot ion flux onto the Cu divertor target plates. As already described in Ref. [13], the Cu production at the target plates for different heating methods with the same heating power is lowest during pure ICRH and maximum during D^0 beam injection.

During the third interval (2.0 - 2.8 s) with $D^0 + \text{ICRH}$, the central Z_{eff} rises to 3.4 owing to a pronounced increase of the metals while the dilution of the deuterium background plasma does not substantially change. The enhancement of the Fe influx

can be explained by a reduced absorption condition for the ICRF waves (H^+ second-harmonic heating) due to a too low H^+ concentration (<20%) (in the case of D^0 -beam heating of the deuterium background plasma). Such effects of impurity enhancement under poor coupling conditions have already been found in previous investigations [14]. The relatively high Cu concentration (about 0.1%) is caused by an increase of sputtering at the Cu divertor target plates, which is always observed during D^0 injection.

5. Parameter scan for the fast analysis method

In order to calculate the dependence of the line intensities of the various ion species on the electron temperature and density an extended scan over the accessible parameter range at ASDEX was performed with our transport code. This scan was made for two different confinement scenarios:

1. Ohmic confinement where the electron density and temperature profiles were taken from a standard ohmic discharge ($n_e = 2.8 \cdot 10^{13} \text{ cm}^{-3}$) and the impurity transport was defined by an anomalous diffusion coefficient of $D(r) = \text{const} = 5000 \text{ cm}^2 \text{ s}^{-1}$ for C and O, $D(r) = 4000 \text{ cm}^2 \text{ s}^{-1}$ for Fe and Cu, and an inward drift velocity $v_{in} = 230 \text{ cm s}^{-1}$ at the plasma edge (with linear decay towards the plasma centre).

2. NBI-heated L-mode confinement where the density and temperature profiles are obtained from a standard L-plasma (1.5-MW NBI heating, $n_e = 3.5 \cdot 10^{13} \text{ cm}^{-3}$). The impurity transport is defined by $D(r) = \text{const} = 9000 \text{ cm}^2 \text{ s}^{-1}$ and $v_{in} = 230 \text{ cm s}^{-1}$ at the plasma edge. As described in section 3 also the change in the ionisation equilibrium due to charge exchange recombination from beam neutrals is taken into account by the code. The electron density and temperature profiles are fitted as explained in section 3.

In the parameter scan the central density was changed from $1 \cdot 10^{13} \text{ cm}^{-3}$ to $8 \cdot 10^{13} \text{ cm}^{-3}$ in steps of $1 \cdot 10^{13} \text{ cm}^{-3}$ by varying the parameter a_{0n} of the fitting function and thus keeping the shape of the profile constant. For the types of discharge

treated by this fast analysis method this is a good approximation of the experimental findings. For each density the central electron temperature was varied from 500 eV to 2500 eV in steps of 500 eV by changing $a_0 T$, again keeping the temperature profile shape constant.

These calculations were performed for the four main impurity species Cu, Fe, O, C. For each element the most prominent line intensities between 10 nm and 110 nm (Cu XIX - 27.4 nm, Fe XVI - 33.6 nm, O VI - 103.2 nm, C III - 31.2 nm, C IV - 38.4 nm) were calculated assuming a central impurity density of $n_z(0) = 10^{10} \text{ cm}^{-3}$ (Fig. 11). We thus obtain a connection between the line intensities I^Z and the central electron density and temperature for a chosen central impurity density ($n_z = 10^{10} \text{ cm}^{-3}$), which can be written as

$$I^Z(n_z) = a_0 n_e(0)^\alpha T_e(0)^\beta.$$

By taking the logarithm of this equation,

$$\ln(I^Z(n_z)) = \ln(a_0) + \alpha \ln(n_e(0)) + \beta \ln(T_e(0)),$$

we obtain a system of linear equations which allows us to calculate the coefficients a_0 , α and β by using a linear regression fit. Tables A and B display these coefficients for the impurity lines which we used in our standard evaluation procedure during the last experimental period. Table A shows the coefficients for the ohmic confinement, while Table B contains those for the NI (and ICRH + NI) heated L-mode discharges. The dimensionless parameters α and β refer to densities measured in units of 10^{13} cm^{-3} and temperatures in eV. The resulting intensity I^Z is obtained in units of W/cm^{-2} for a reference impurity density $n_z = 10^{10} \text{ cm}^{-3}$.

These relations are specified for ASDEX. Conversion to other devices may be done in an approximate manner by scaling proportionally to the minor radius ($a^{\text{ASDEX}} = 40 \text{ cm}$).

The intensities calculated by the above formula reproduce the original output data of the ZEDIFF code (Fig. 11). Only at the

extreme end of the parameter space (high n_e , low T_e) is there a slight disagreement for oxygen.

TABLE A OH phase

	a0	α	β
CIV(38.4 nm)	1.23489E-04	-6.07842E-02	0.67096
CIV(31.2 nm)	4.41958E-05	-2.43723E-02	0.73708
OVI(103.2 nm)	8.05289E-02	-6.44150E-01	0.69764
FeXVI(33.6 nm)	2.42990E+04	-2.28610E+00	1.01100
CuXIX(27.4 nm)	7.20770E+04	-2.37700E+00	1.08610

TABLE B L-mode of NI phase

	a0	α	β
CIV(38.4 nm)	4.94827E-04	-1.59560E-01	0.55072
CIV(31.2 nm)	2.44254E-04	-1.19710E-01	0.53148
OVI(103.2 nm)	2.29749E-01	-7.25170E-01	0.58814
FeXVI(33.6 nm)	1.01610E+04	-2.06000E+00	0.85478
CuXIX(27.4 nm)	2.67720E+04	-2.12860E+00	0.87407

In order to assess the central impurity densities for a particular discharge, we need to compare the intensities calculated by the above-described formula with the absolutely measured line intensities obtained from the VUV SPRED spectrometer.

$$n_z(0) = \frac{I_{\text{SPRED}}^z}{I_{\text{calc.}}^z} 10^{10} [\text{cm}^{-3}]$$

These calculations are performed time-dependently for the four main impurities immediately after each discharge. In addition to the individual concentrations, we calculate their contributions to the total $Z_{\text{eff}}(0,t)$ by introducing an effective charge state (in the plasma centre) for each ion species:

$$Z_{\text{eff}}(0) = \sum_{I=1}^5 \frac{n_I(0)}{n_e(0)} Z_I^2,$$

where $Z_2 = 6$ (C) ; $Z_3 = 8$ (O) ; $Z_4 = 22$ (Fe) ; $Z_5 = 24$ (Cu) .
 This simple approach can be justified as follows. For the bulk part of the parameter space considered the given numbers for the charge state are correct (see Fig. 5). At high density and low temperature the metallic concentration is very low and practically does not contribute to Z_{eff} . On the other hand, the light impurities are still completely stripped in the central plasma under these conditions. Conversely, in low-density, high temperature discharges the metallic contribution to Z_{eff} can be substantial. In these cases, however, the above-listed charge states again agree approximately with the true ones and it should be noted that small changes (+2) in the charge states of the metallic impurities do not have a big effect on Z_{eff} .

6. Application and discussion

The above-described fast method was applied to all discharges in the last experimental campaign. Reliable results, however, can only be expected for OH and L-type discharges, for which our parametrisation procedure is adequate. Below, we discuss the impurity concentrations and their contribution to Z_{eff} for a number of representative discharges under carbonised wall conditions.

Ohmic heating:

Several density scans covering almost the whole parametrised density and temperature ranges were made on ASDEX. The dependences of the central concentrations of O and C on $n_e(0)$ are displayed in Fig. 12a. In this case we observe a nearly inverse linear dependence of the light impurity concentration on the electron density. This dependence is more pronounced for carbon than for oxygen, resulting in twice as much carbon (4%) as oxygen (2%) at low densities ($2 \cdot 10^{13} \text{cm}^{-3}$). The metallic impurity concentration (Fig. 12b), on the other hand, shows almost no dependence on $n_e(0)$ above $3.5 \cdot 10^{13} \text{cm}^{-3}$ but increases nearly exponentially towards lower densities. This

behaviour reflects sputtering and retention within the ASDEX divertor [13]. It should be pointed out that practically 100% of the Cu influx and approximately 30 to 50% of the Fe influx is produced in the non-carbonised divertor chambers [15]. This explains why the contribution of Cu to Z_{eff} at low densities ($2 \cdot 10^{13} \text{ cm}^{-3}$) becomes as important as that of oxygen or carbon. The dependence of Z_{eff} on n_e and the dilution of the deuterons are shown in Fig. 12c.

Furthermore, the spectroscopic Z_{eff} is compared with the bremsstrahlung Z_{eff} . The overall agreement is rather good; only at low densities does the spectroscopic Z_{eff} seem to be systematically higher than the bremsstrahlung Z_{eff} . This tendency can only be partly explained by the poorer fit quality in this range (Fig. 11). In addition, however, also the increasing uncertainty in n_e must be kept in mind: at higher temperatures and low n_e the positions of the radiating shells of C IV and O VI are shifted outwards into the region of strong density gradients.

Additionally heated L-discharges:

The fast analysis could also be applied to L-discharges with neutral beam heating (H^0 or D^0) and during combined beam (1.2 MW) and ICRF (2 MW) heating.

Figure 13a shows the time dependence of the Z_{eff} contributions and the D^+ dilution for a beam-heated (1.2 MW) L-mode discharge. There is a first heating period (0.8 - 1.7 s) with 1.0-MW with H^0 beams and a second one (2.0 - 2.9 s) with 1.2-MW D^0 beam injection. During the first period the moderate increase of Z_{eff} (1.7 to 2.2) is mainly caused by an increase of carbon and Cu. This behaviour is consistent with the observed enhancement of wall erosion during neutral beam heating. In the second D^0 heating period applied Z_{eff} increases to a value exceeding 3, with contributions from all four impurities (Fig. 3a). In agreement with previous results [13] the D^0 beams seem to cause much higher wall erosion than the H^0 beams. The dilution of D^+ in the second heating interval turns out to be already 35%, mainly owing to the relatively high concentration of light impurities ($\text{C} + \text{O} = 2.9\%$).

The case of combined heating (beams and ICRH) has already been treated in section 4. The fast analysis results plotted in Fig. 13b are seen to reproduce neatly the results obtained from the extended ZEDIFF code simulation.

The dependence of δ_{eff} on n_g and the diffusion of the electrons are shown in Fig. 13a. The overall agreement is rather good, but at low densities does not agree with the spectroscopic data. This tendency can only be partly explained by the poorer fit in this range (Fig. 11). In addition, however, since the increasing uncertainty in n_g must be kept in mind at higher temperatures and for n_g the positions of the radiating shells of

O IV and O VI are shifted towards larger radii, and the density gradient.

Additional heated discharges

The fast analysis code also handled the discharges with neutral beam heating (H₀ and D⁺) and during combined beam (H₀ and ICRH) and ICRH (2 MW) heating. The time dependence of the δ_{eff} coefficient and the D⁺ diffusion for a beam-heated (1.2 MW) I-mode discharge. There is a first heating period (0.8 - 1.7 s) with 1.0-MW with H₀ beams and a second one (2.0 - 2.9 s) with 1.0-MW beam injection. During the first period the amplitude increased at 1.7 to 2.2) and was analysed by an increase of carbon and O VI. This behaviour is consistent with the observed enhancement of a wall erosion during neutral beam heating. In the second heating period applied δ_{eff} increases to a value exceeding 3% with corresponding temperature fluctuations. In the case agreement with previous results in the H₀ beams case, much higher wall erosion than the H₀ beams. The diffusion of the second heating interval turns out to be slightly larger than the first heating interval. The relative concentration of

References

- [1] K. H. Behringer, private communication
- [2] B. C. Stratton, R. J. Fonck, K. Ida et al.,
Rev. Sci. Instr. 57 (1986), 2043
- [3] R. D. Wood, S. L. Allen, Proceedings 7th Topical Conference
on High Temperature Plasma Diagnostics, Napa, California,
March 1987. (Report UCRL 98278)
- [4] W. Pöffel, K.-H. Schartner, Report: "Linienquelle im VUV zur
Bestimmung der Nachweiswahrscheinlichkeit des 1 m normal-
incidence Spectrometers an ASDEX" (1987), (to be published)
I. Physikalisches Institut der Justus Liebig Universität,
D-6300 Giessen.
- [5] K. H. Schartner, B. Kraus, W. Pöffel et. al., Nucl. Inst.
and Meth. B27 (1987), 513-526
- [6] K. Danzmann, M. Guenther, J. Fischer, M. Kock, M. Kühne
Applied Optics 27, No.23 (1988), 4947-4951
- [7] K. Behringer, JET report: JET-R(87)08
- [8] H. Röhr, K.-H. Steuer, H. Murmann, D. Meisel, Rev. Sci. Instr.
59 (8), (1988), 1875-1877
- [9] G. Fussmann, J. Hofmann, G. Janeschitz et al., J. Nucl.
Materials, 162-164 (1989) 14-23
- [10] K. Lackner, U. Ditte, G. Fussmann, et al. Proc. 10th int.
Conf. on Plasma Phys. and Contr. Nucl. Fusion Research,
IAEA, Vol. I (1985), 319-327
- [11] G. Janeschitz, G. Fussmann, B. P. Kotze et. al.,
Nucl. Fusion, Vol. 26, No. 12, (1986)
- [12] H. Röhr, K.-H. Steuer, Rev. Sci. Instr. 59, No. 8 (1988)
- [13] G. Janeschitz, G. Fussmann, J. Hofmann, et. al., J. Nucl.
Mater. 162-164 (1989) 624-628
- [14] G. Janeschitz G. Fussmann, J. M. Noterdame et al., Proc. of
the 13th EPS- conference Schliersee 1986, Voll, p. 407
- [15] J. Roth, G. Janeschitz, Nucl. Fusion Vol. 29, No. 6 (1989)
915-935

Figure Captions.

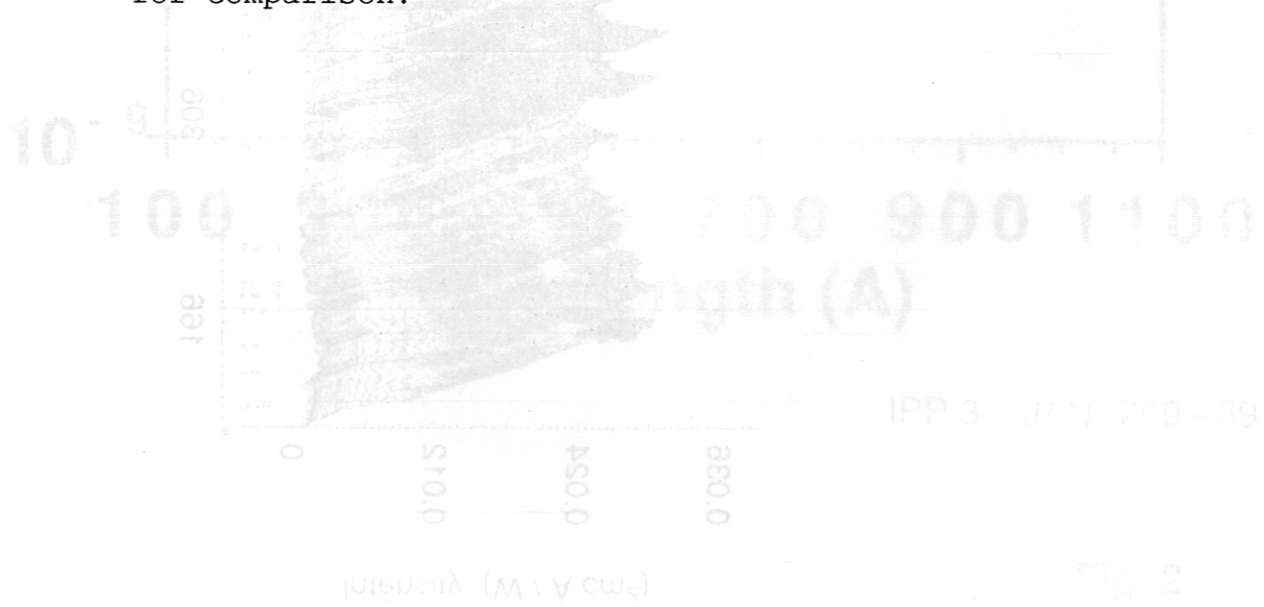
- Fig. 1: Time dependence of the spectrum in the range from 10 nm to 110 nm measured by the ASDEX SPRED spectrometer during a combined NI and ICRF-heated (0.8 to 2.8 s) discharge.
- Fig. 2: Calibration curve of the SPRED spectrometer taking into account the solid angle of the setup on ASDEX for direct comparison with transport code results.
- Fig. 3: Time dependence of the electron density (a) and the electron temperature (b) profiles during a combined NI and ICRF-heated discharge.
- Fig. 4: Time dependence of the concentration profiles of C, O, Fe, Cu for a combined NI and ICRF-heated discharge.
- Fig. 5: Calculated charge profiles of C, O, Fe, Cu vs time for a combined NI and ICRF-heated discharge.
- Fig. 6: Time dependence of the calculated line radiation profiles of C IV (38.4 nm), O VI (103.2 nm), FeXVI(33.5nm), Cu XIX (27.3 nm) for a combined NI and ICRF-heated discharge.
- Fig. 7: Spectroscopic Z_{eff} profile (a) and the deuteron density profile (b) for a combined NI and ICRF-heated discharge as a function of time.
- Fig. 8: Time dependence of the Z_{eff} profile measured by the bremsstrahlung diagnostic for a combined NI and ICRF-heated discharge.
- Fig. 9: Time dependence of the Z_{eff} contributions of C, O, Fe, Cu as well as the dilution of the deuterium background plasma for a combined NI and ICRF-heated discharge.

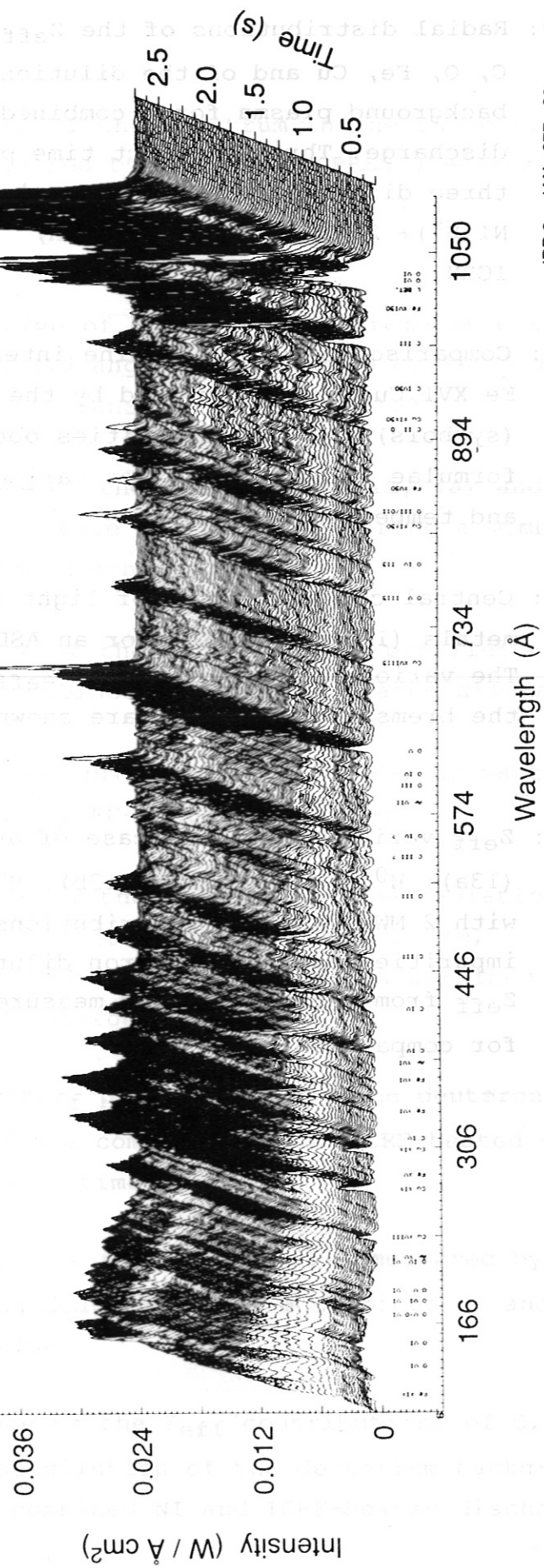
Fig. 10: Radial distributions of the Z_{eff} contributions made by C, O, Fe, Cu and of the dilution of the deuterium background plasma for a combined NI and ICRF-heated discharge. Three distinct time points representing three different heating scenarios are displayed: 1.2 MW NI(H^0)+ 2 MW ICRH, 2 MW ICRH, 1.2 MW NI(D^0)+ 2 MW ICRH.

Fig. 11: Comparison between the line intensities (C IV, O VI, Fe XVI, Cu XIX) calculated by the ZEDIFF transport code (symbols) and the intensities obtained from the fit formulae (solid lines) for various electron densities and temperatures.

Fig. 12: Central concentrations of light impurities (12a) and metals (12b) vs. $n_e(0)$ for an ASDEX ohmic discharge. The various contributions to Z_{eff} and a comparison with the bremsstrahlung Z_{eff} are shown in (12c).

Fig. 13: Z_{eff} variations in the case of auxiliary heating. (13a): H^0 and D^0 beams, (13b): H^0 and D^0 beams combined with 2 MW ICRH. The contributions of the four main impurities and the deuteron dilution (D^+) are indicated. Z_{eff} from bremsstrahlung measurements is also shown for comparison.

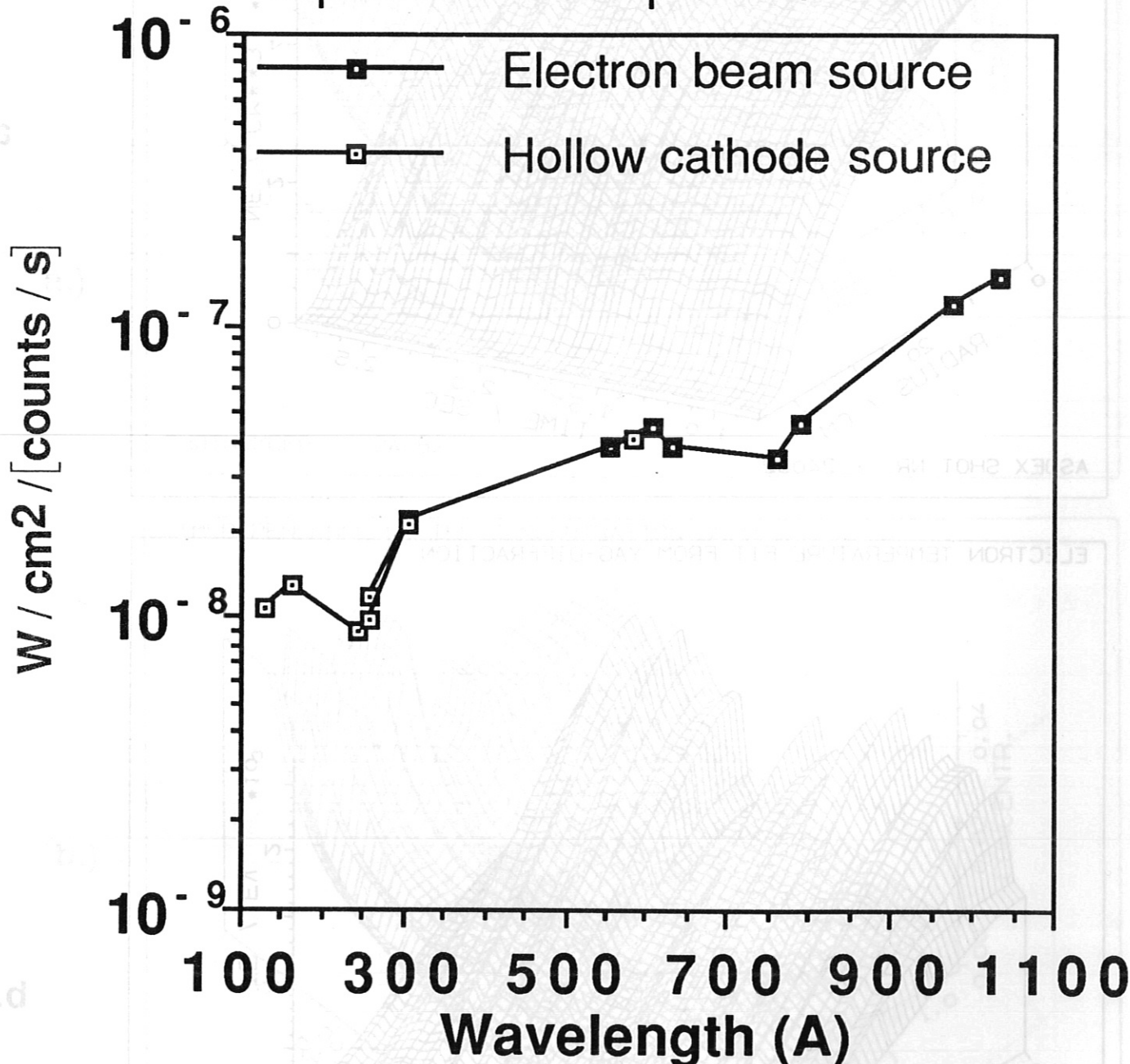




IPP 3 JAN 277 - 89

Fig. 1

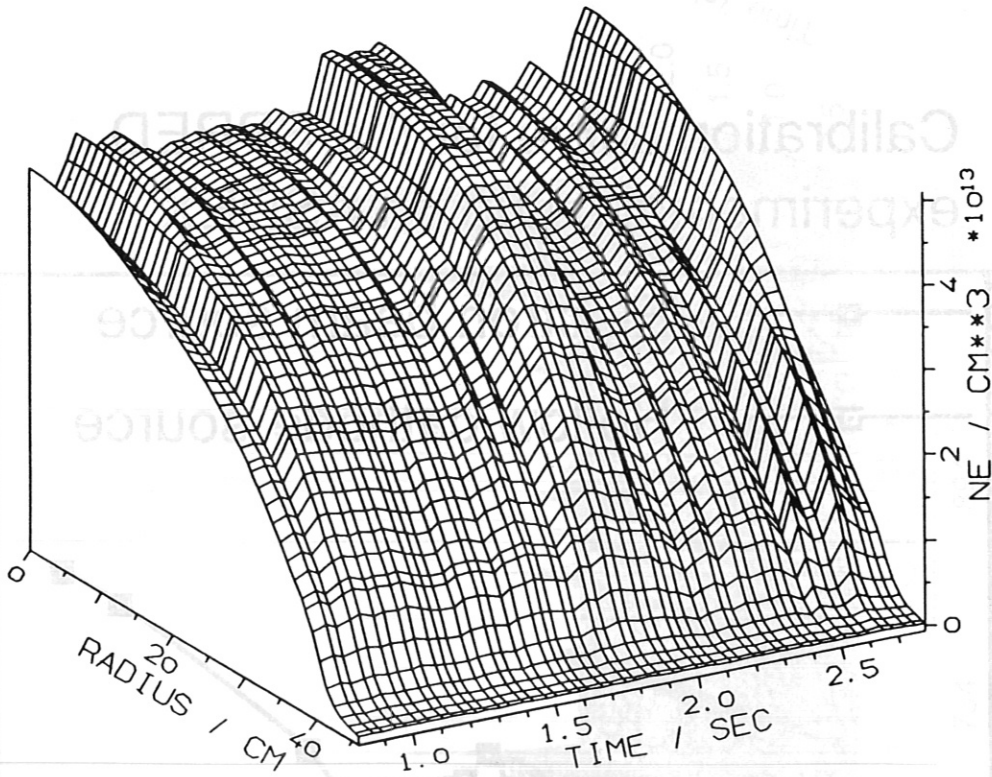
Calibration curve for the SPRED experimental setup on ASDEX



IPP 3 JAN 269 - 89

Fig. 2

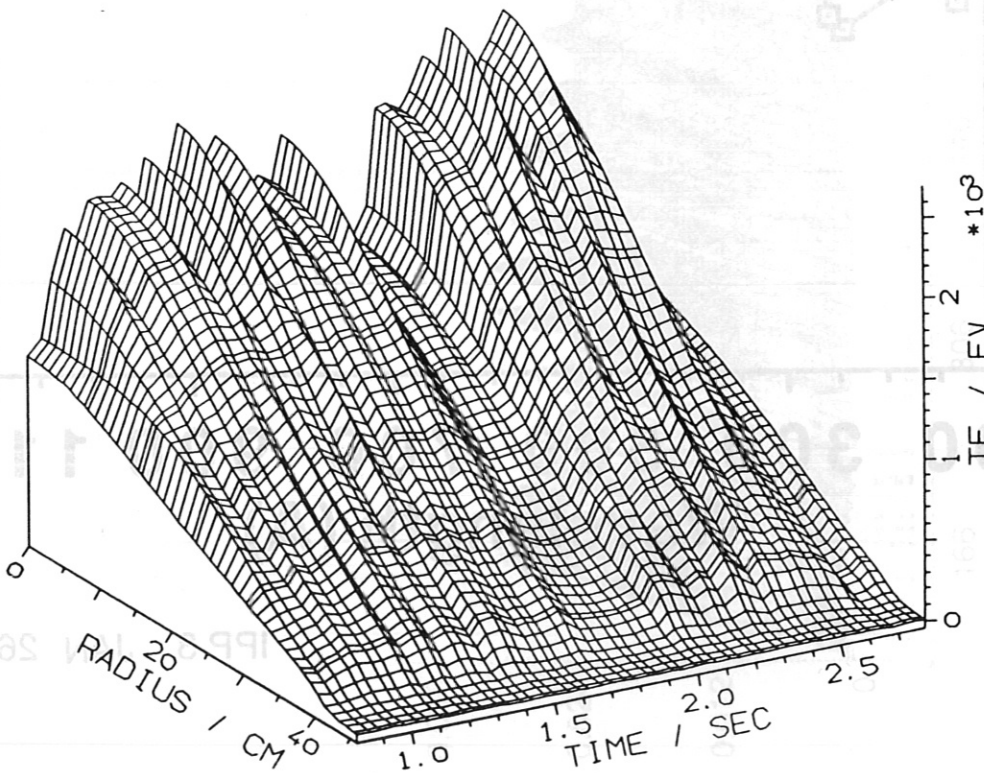
ELECTRON DENSITY FIT FROM YAG-DIFFRACTION



ASDEX SHOT NR. : 24082

a.)

ELECTRON TEMPERATURE FIT FROM YAG-DIFFRACTION



ASDEX SHOT NR. : 24082

b.)

IPP 3 JAN 266 - 89

Fig. 3

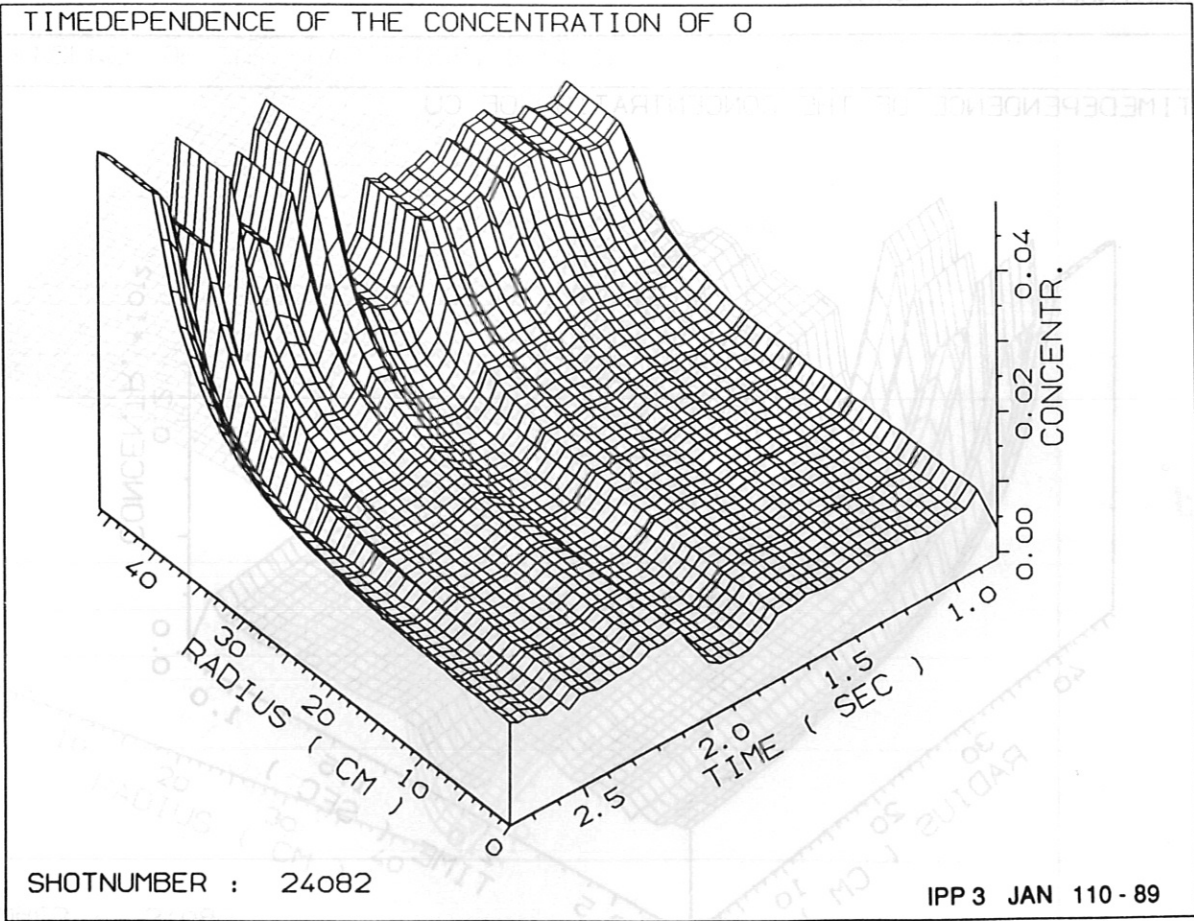
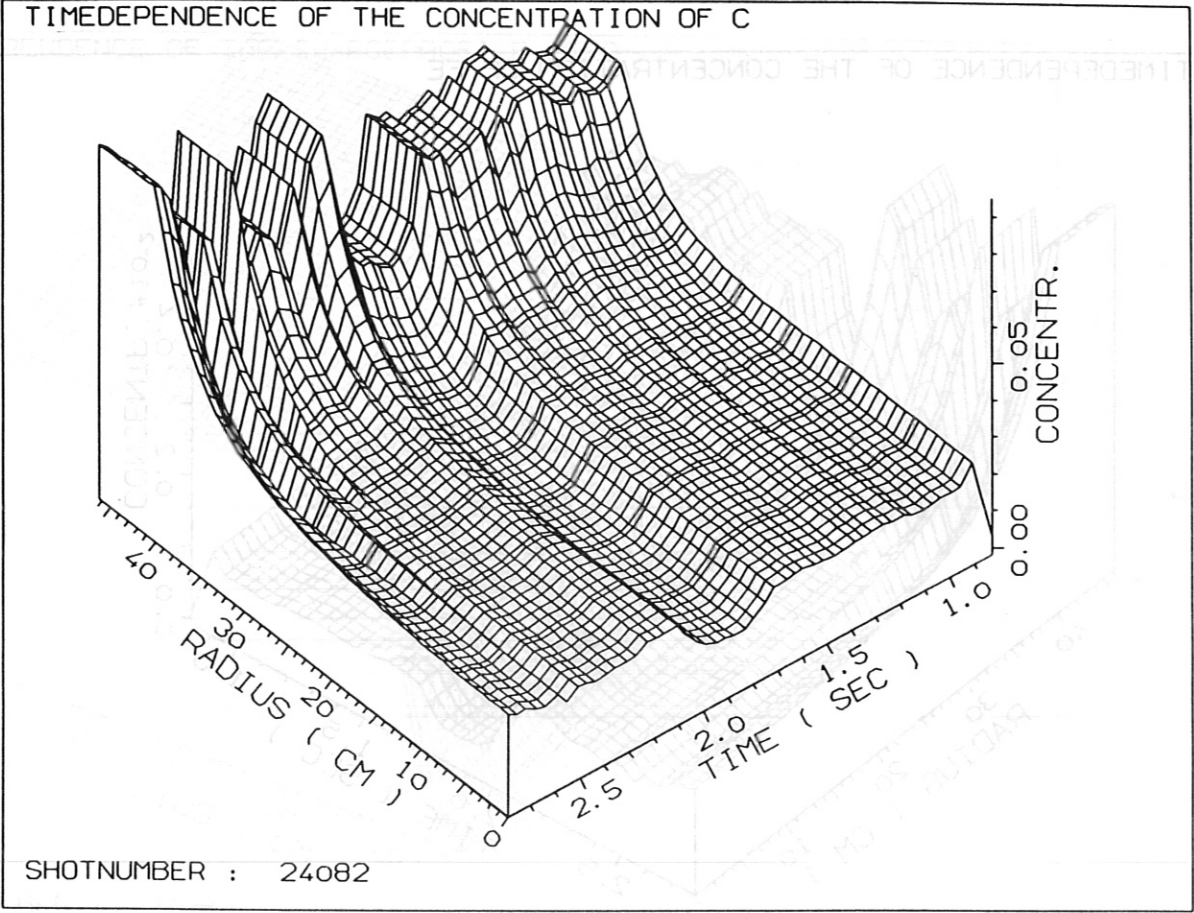
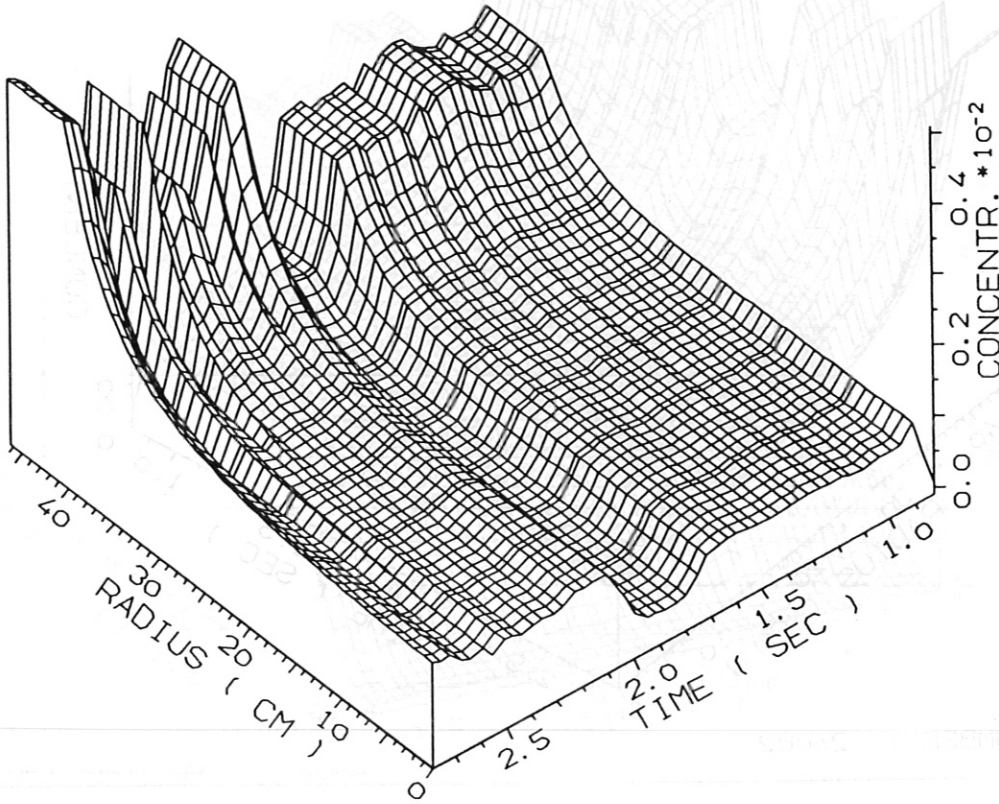


Fig. 4

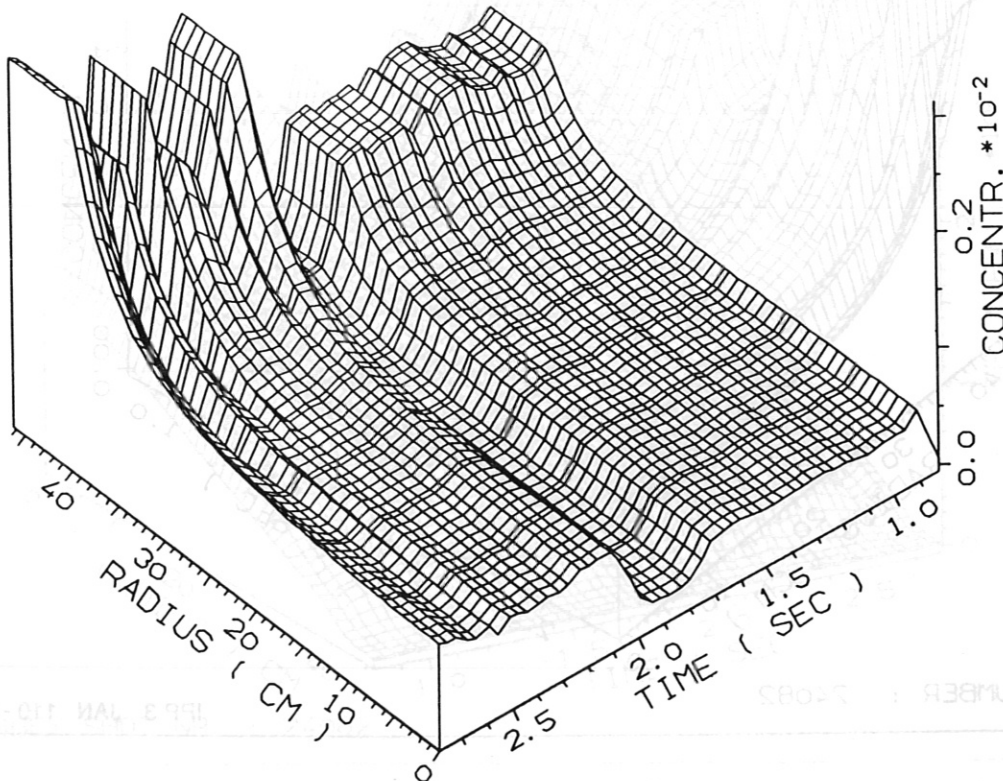
TIMEDEPENDENCE OF THE CONCENTRATION OF FE



SHOTNUMBER : 24082

c.)

TIMEDEPENDENCE OF THE CONCENTRATION OF CU



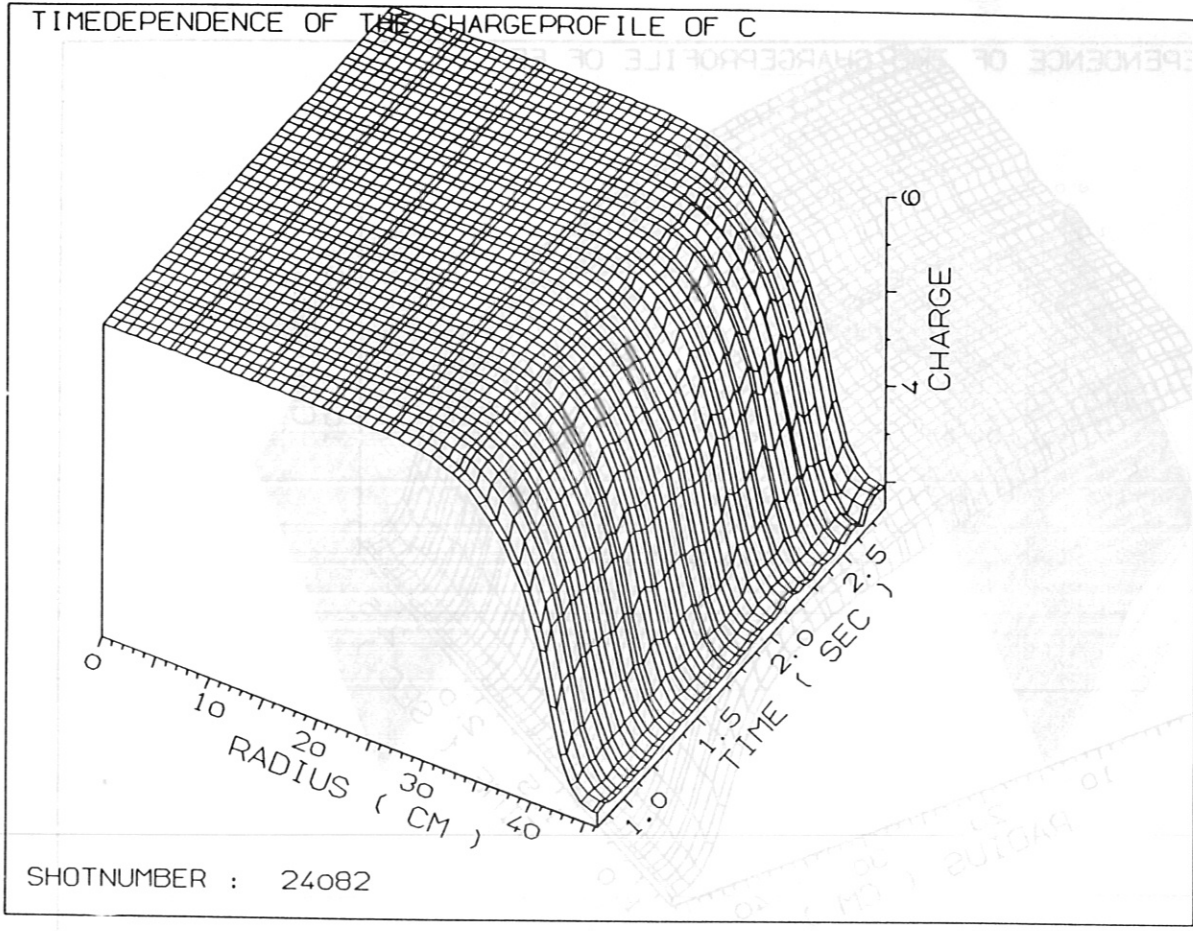
SHOTNUMBER : 24082

IPP 3 JAN 111 - 89

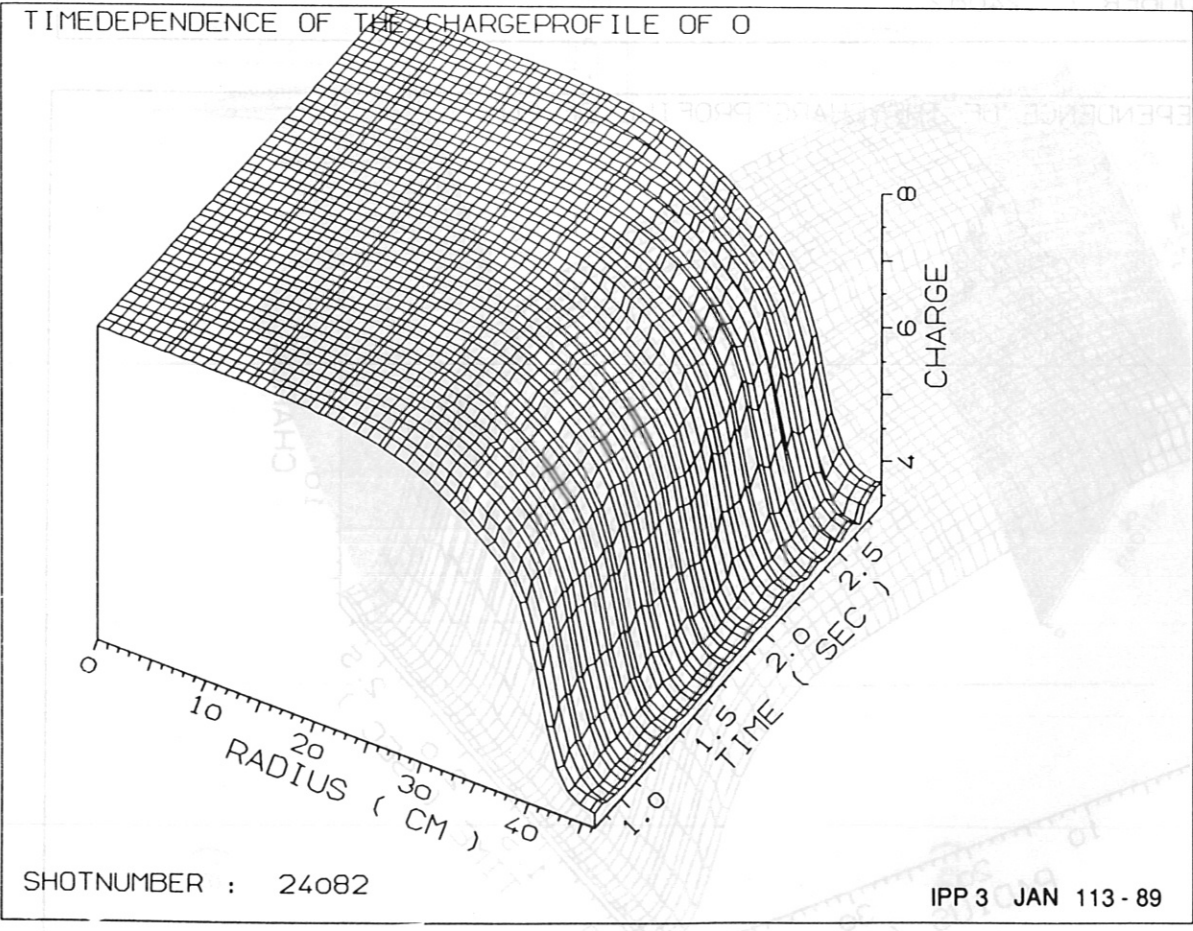
d.)

Fig. 4

Fig. 3

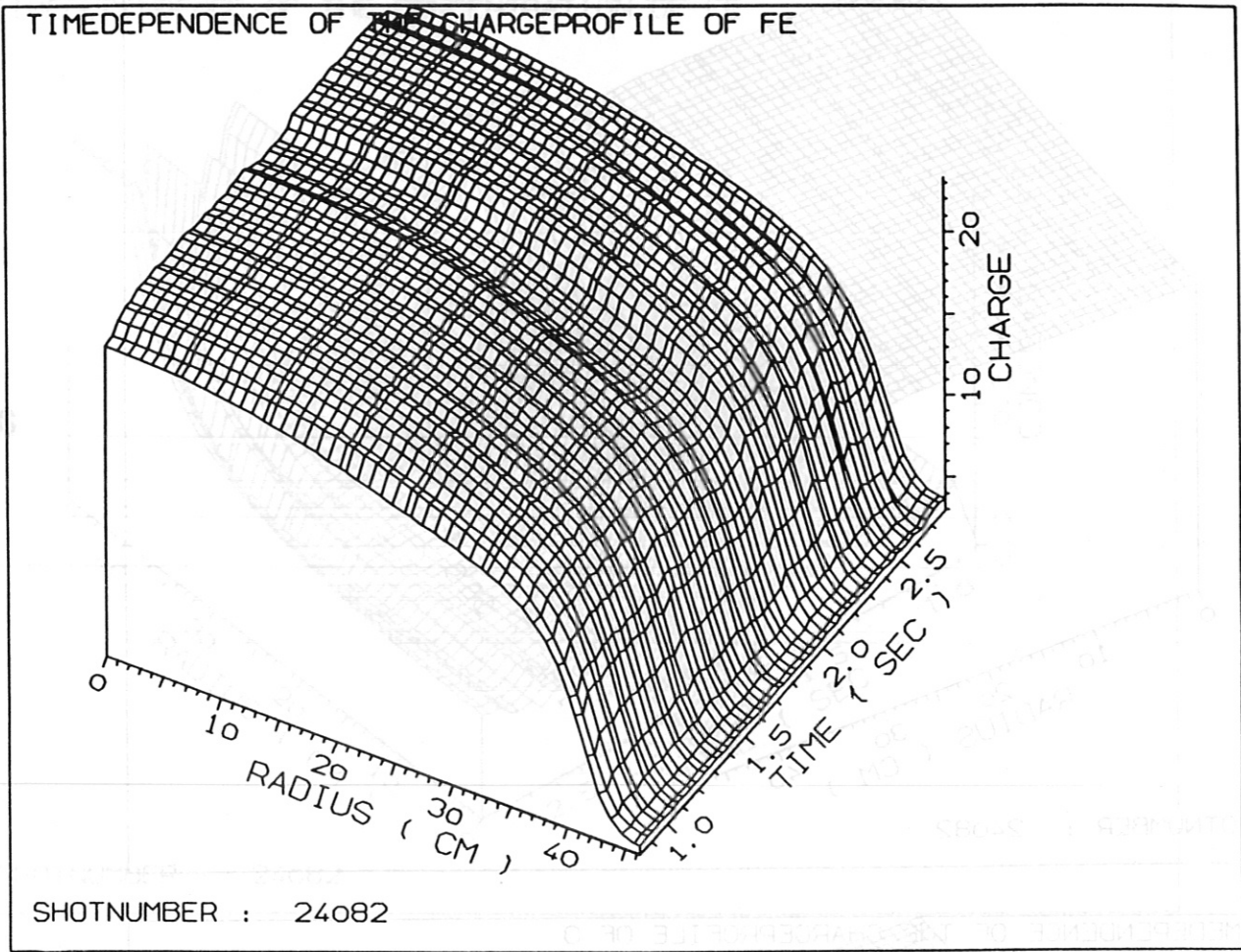


a.)

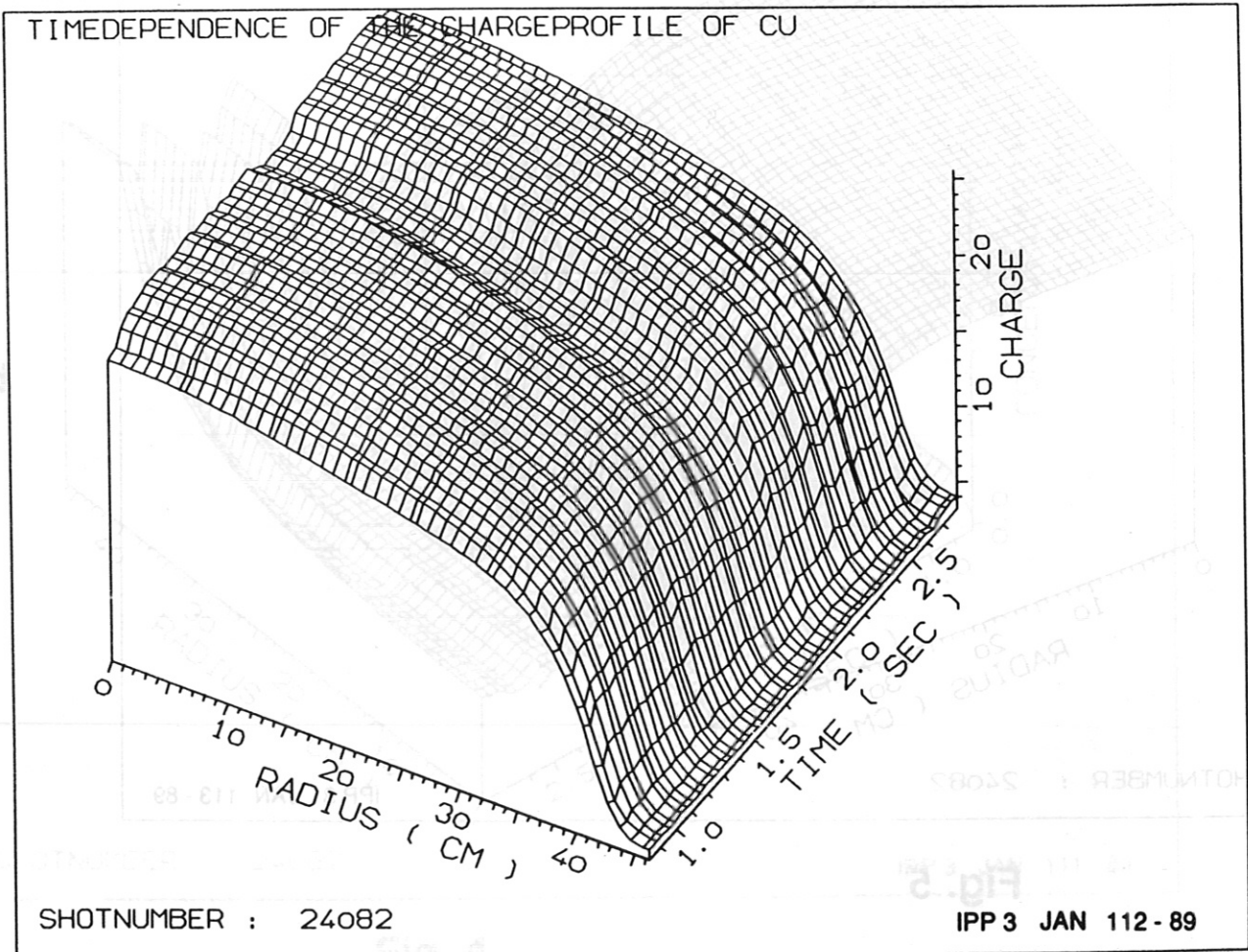


b.)

Fig. 5

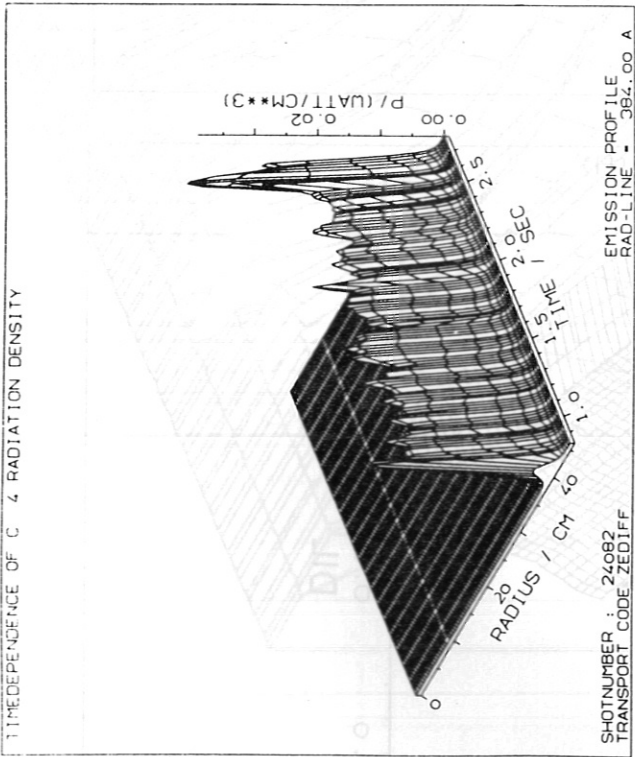


c.)

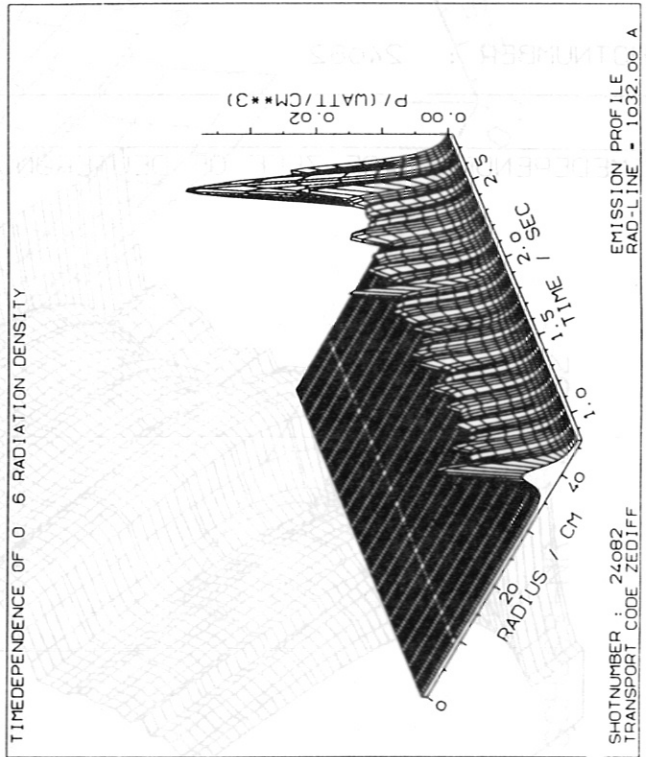


d.)

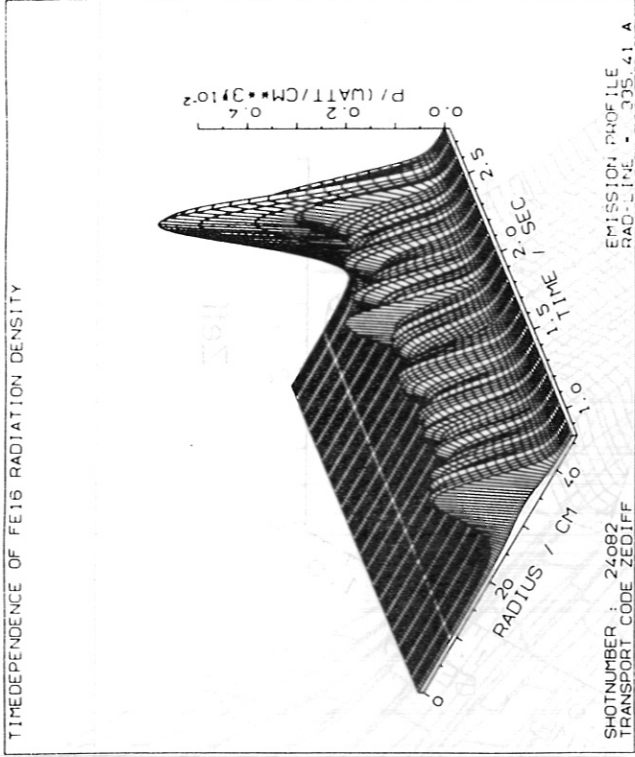
Fig. 5



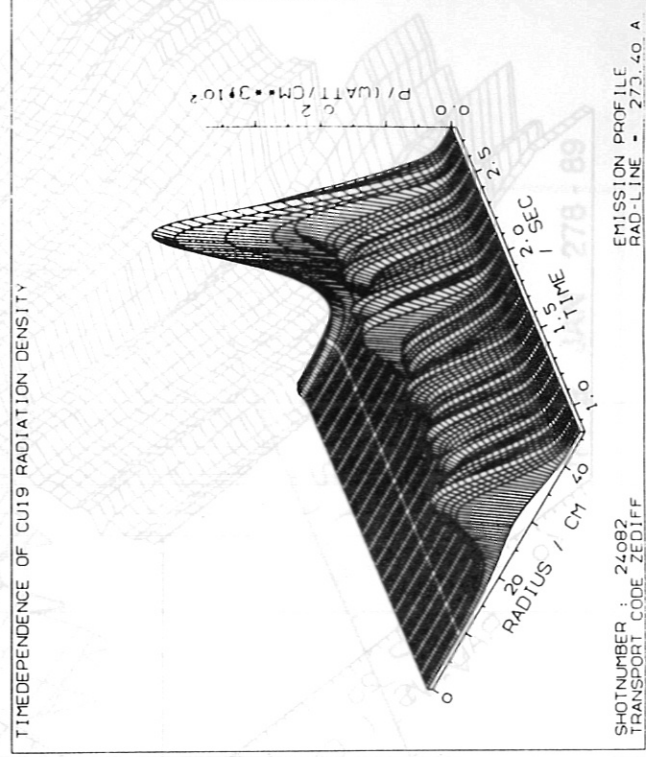
a.)



b.)

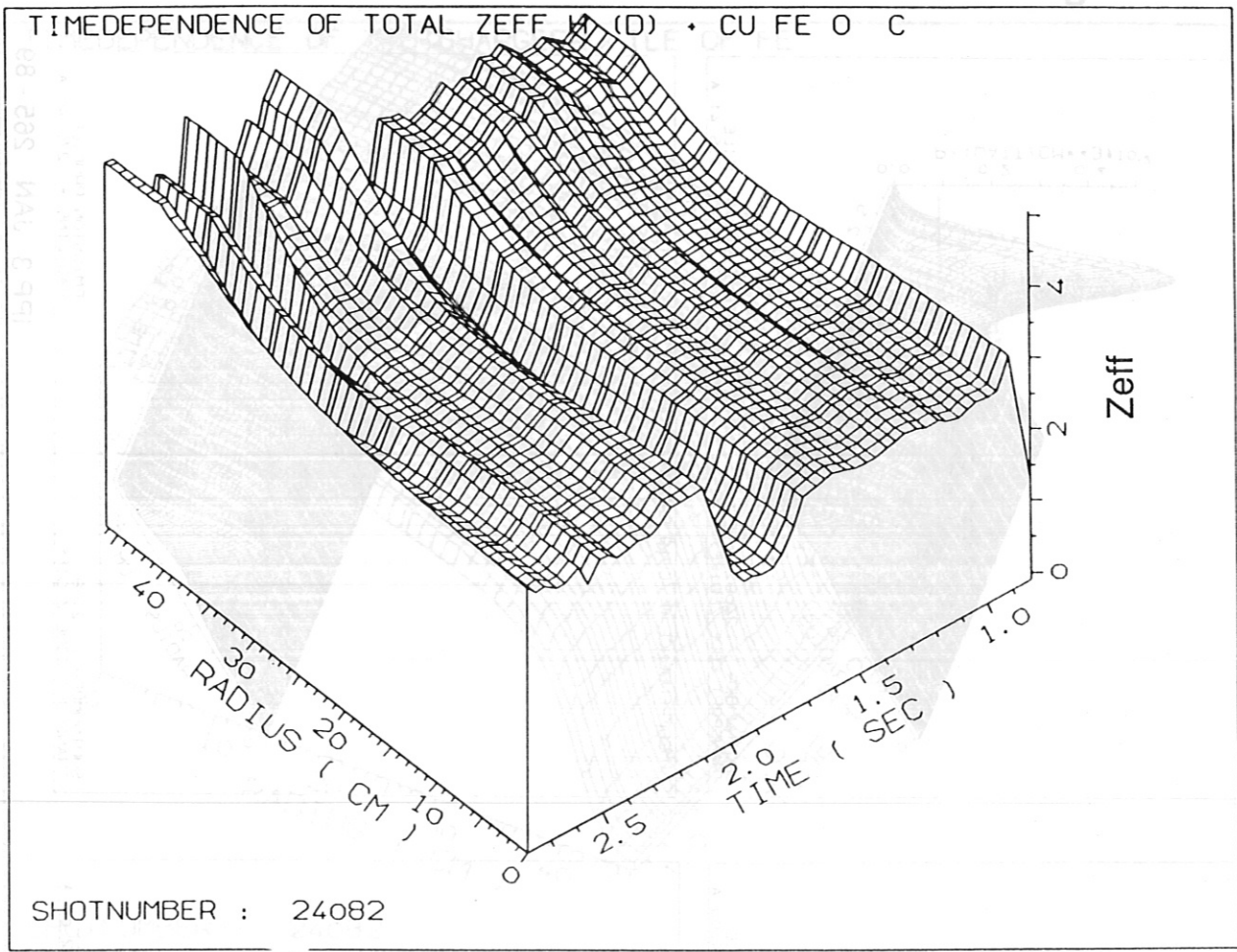


c.)

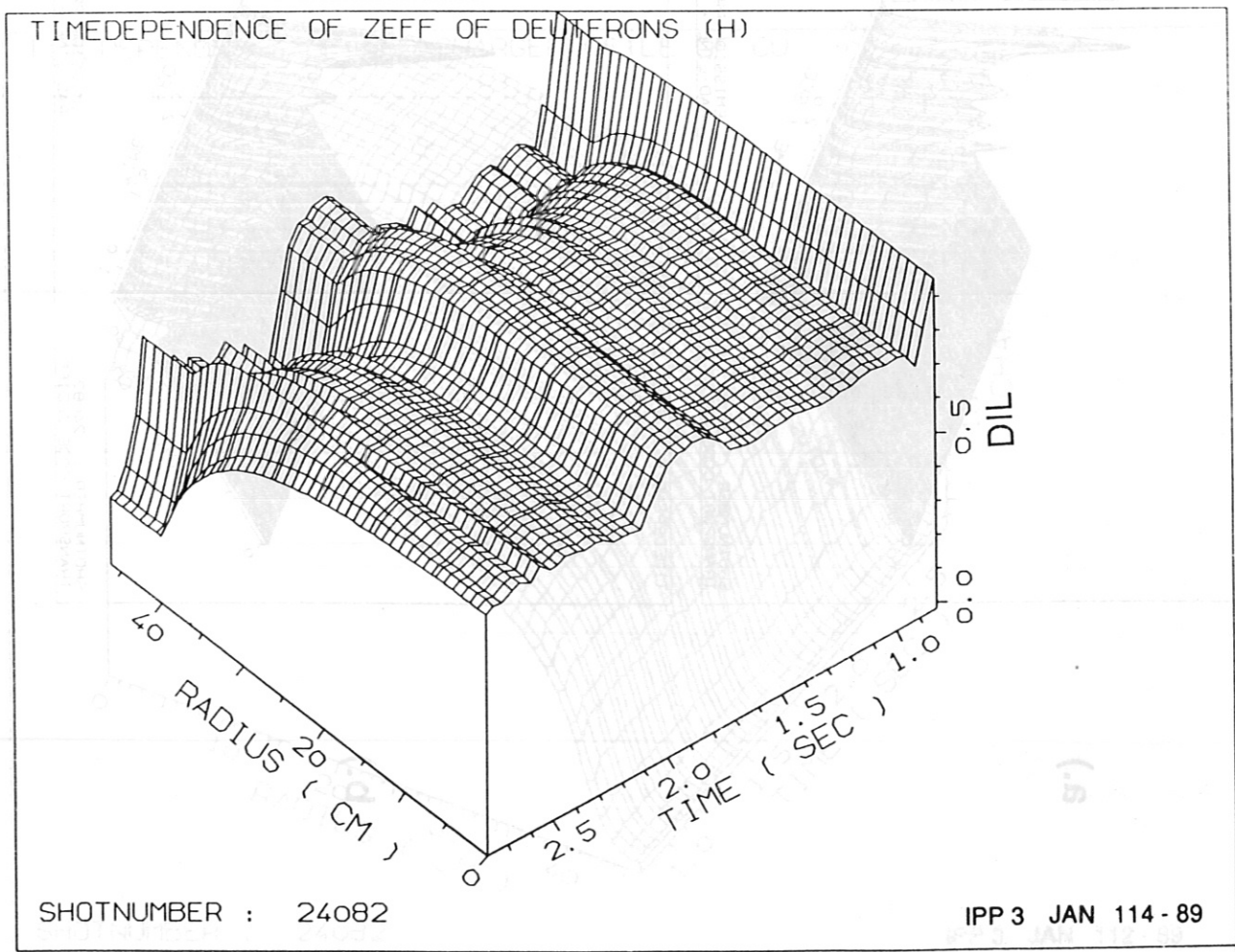


d.)

Fig. 6



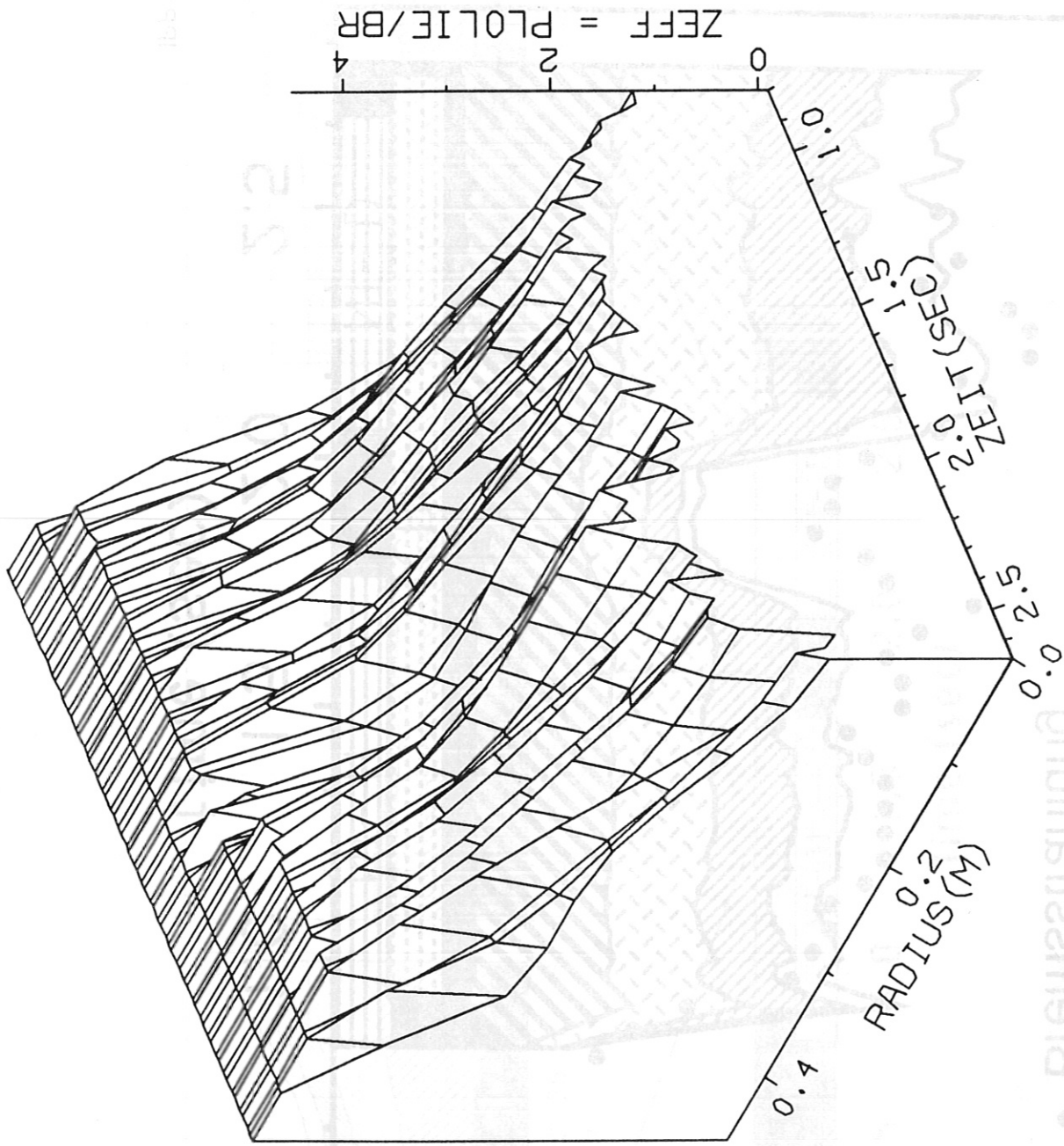
a.)



b.)

Fig. 7

Fig. 5



SCHUSS-NR: 24082

IPP 3 JAN 278 - 89

Fig. 10

Fig. 8

Central Zeff contributions vs. time

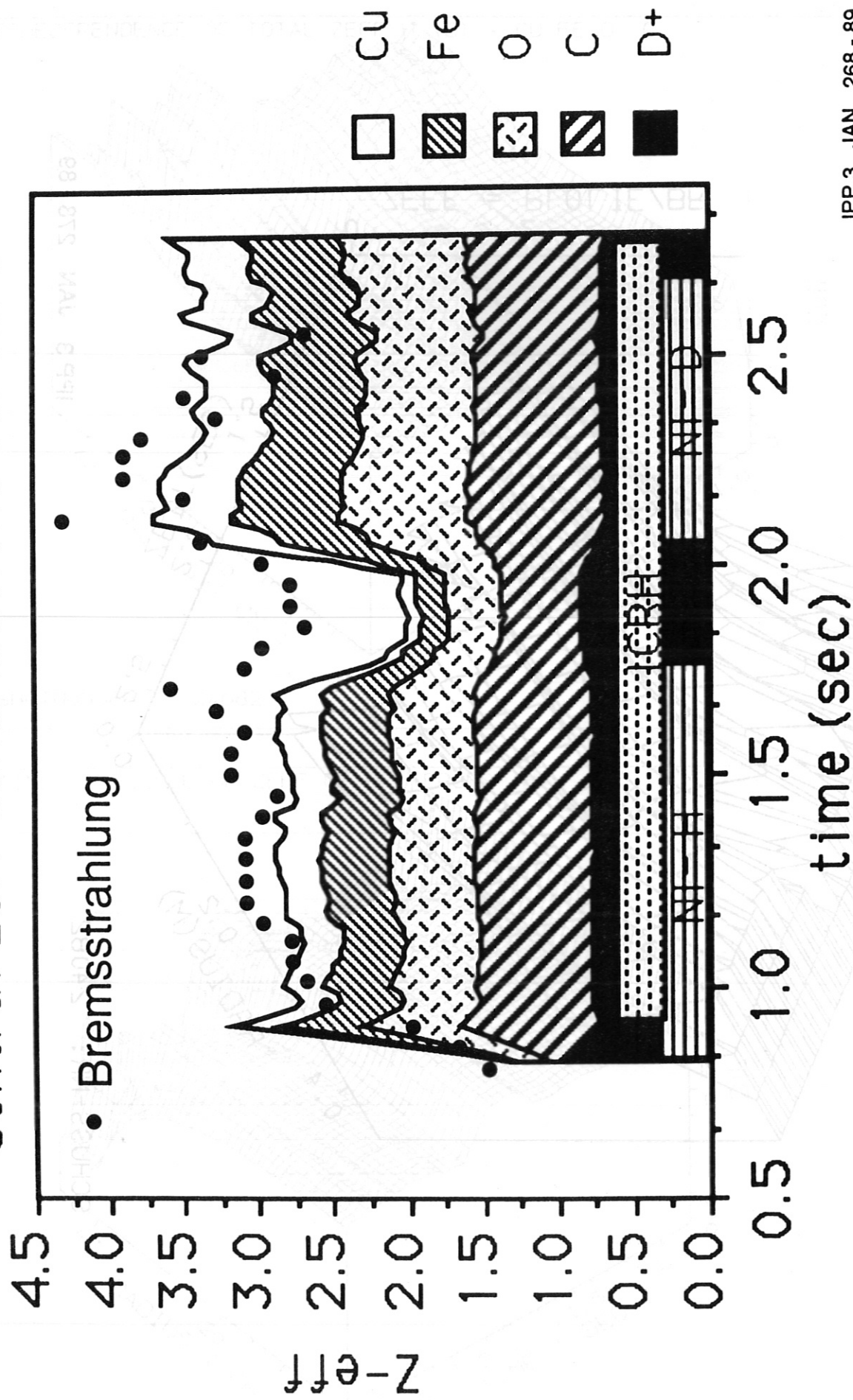
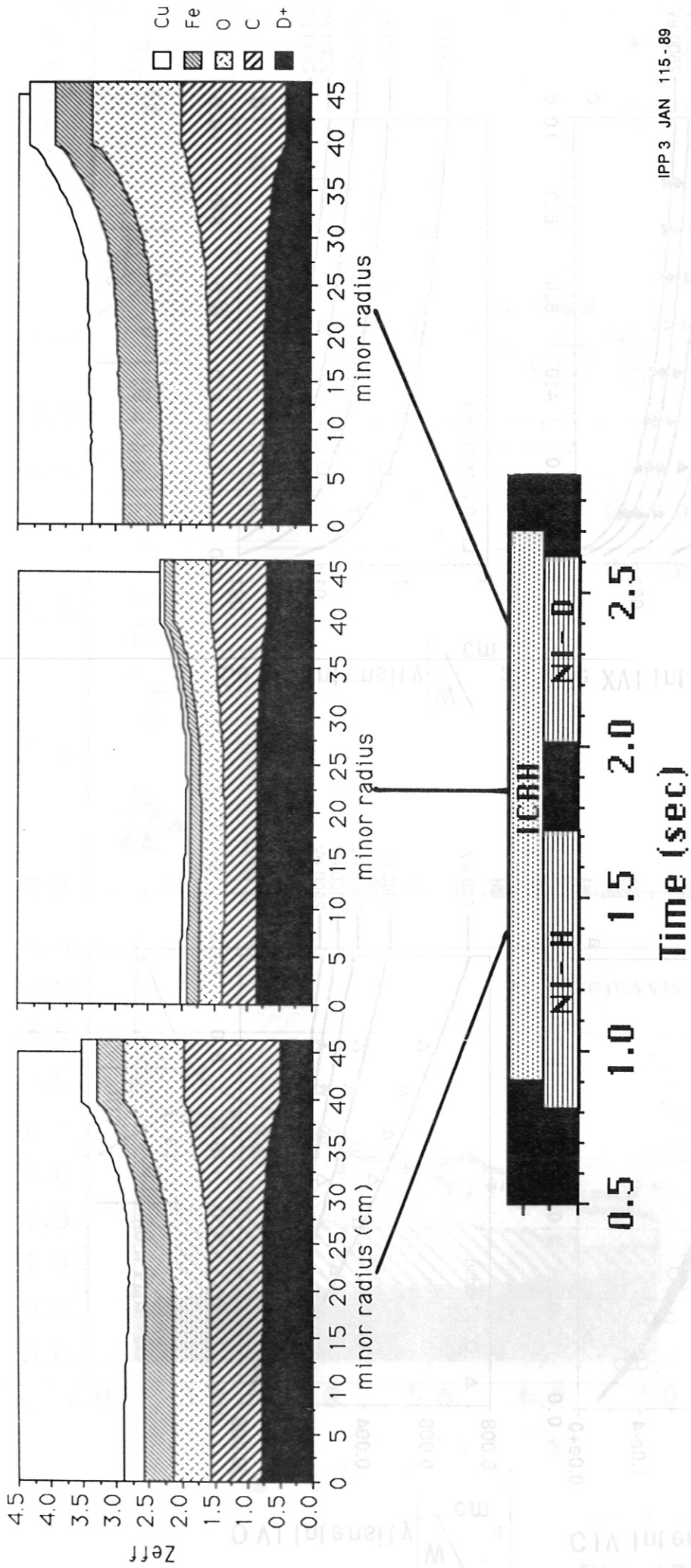


Fig. 9



IPP 3 JAN 115-89

Fig. 10

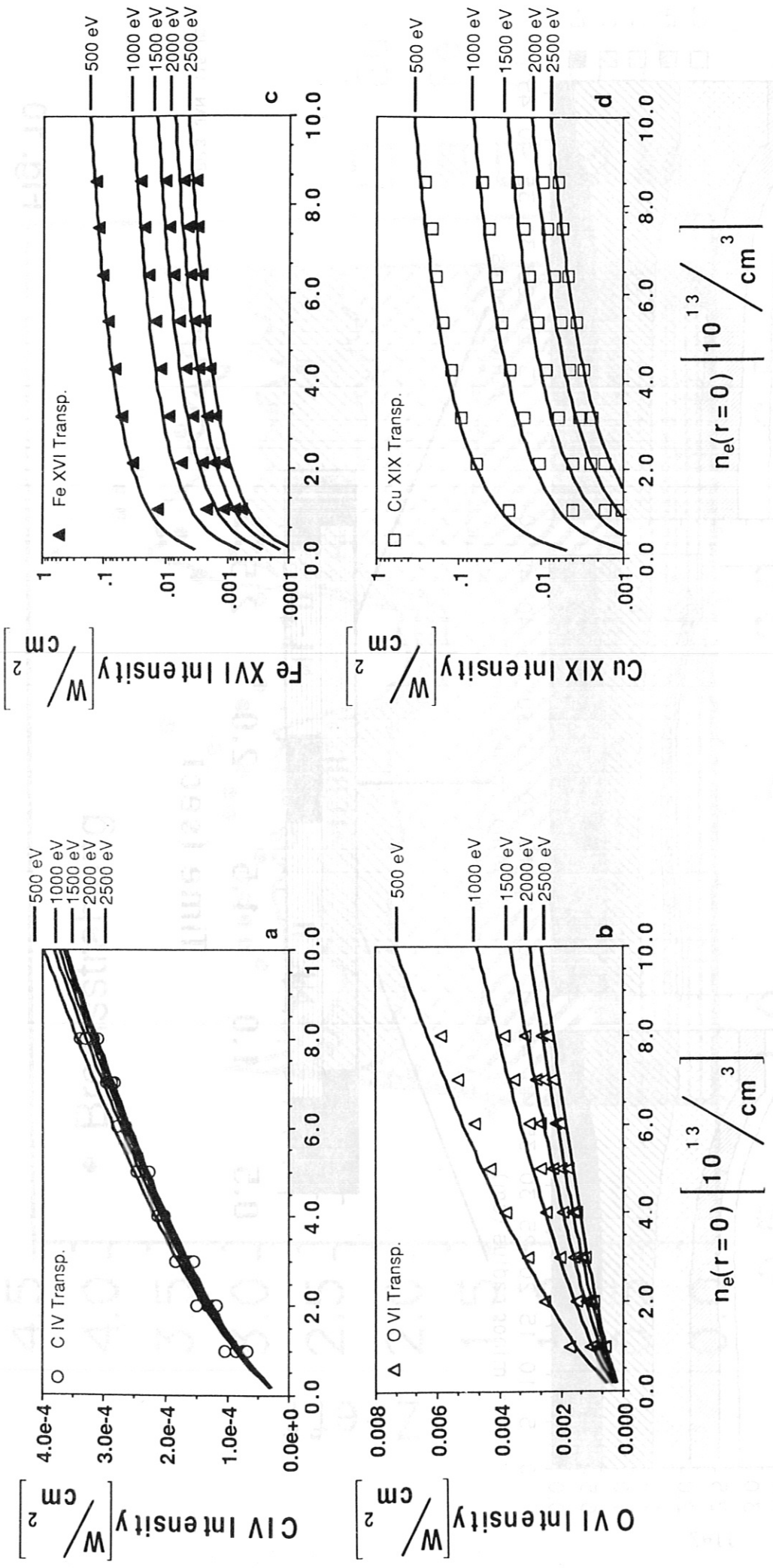


Fig. 11

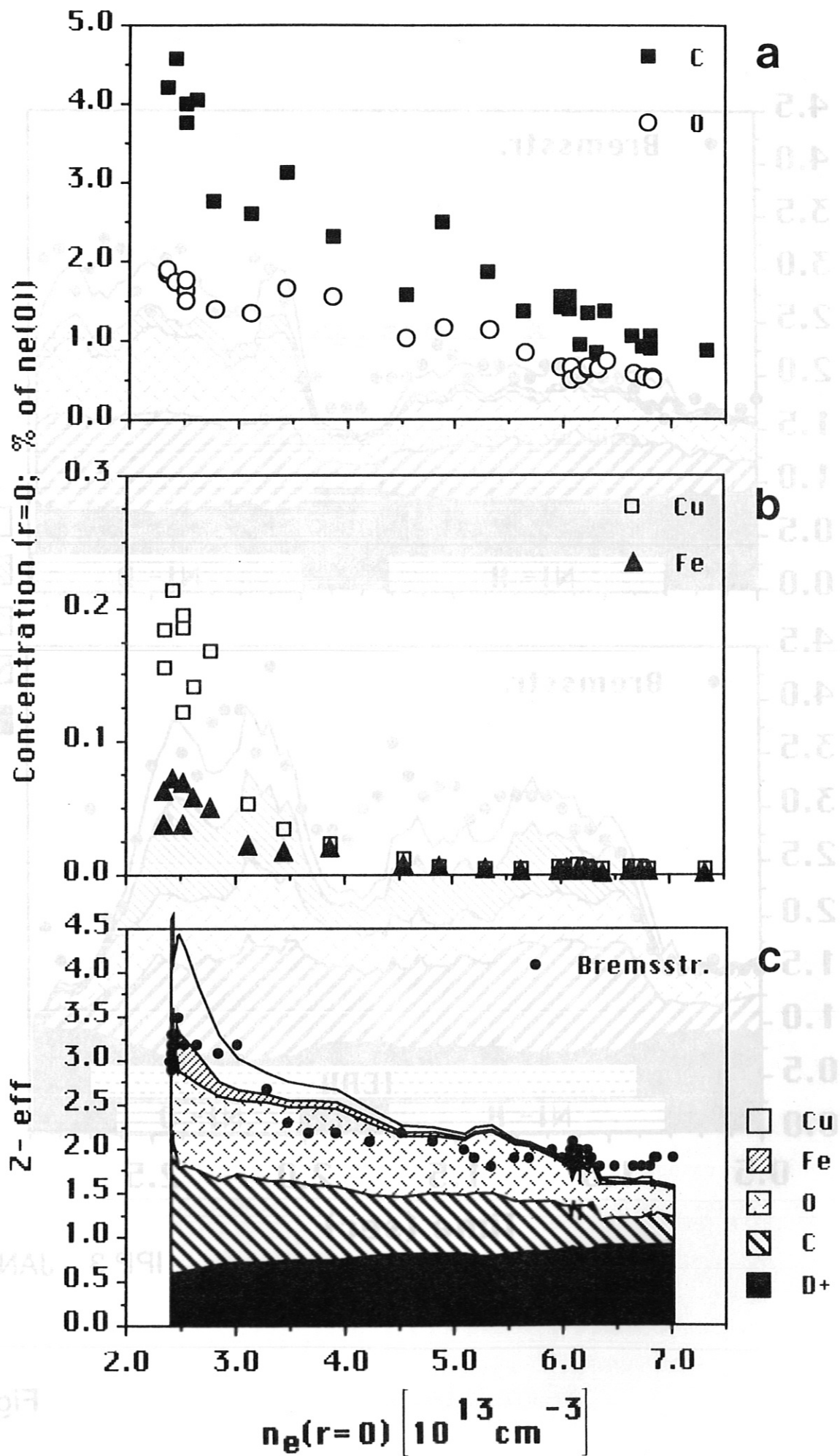
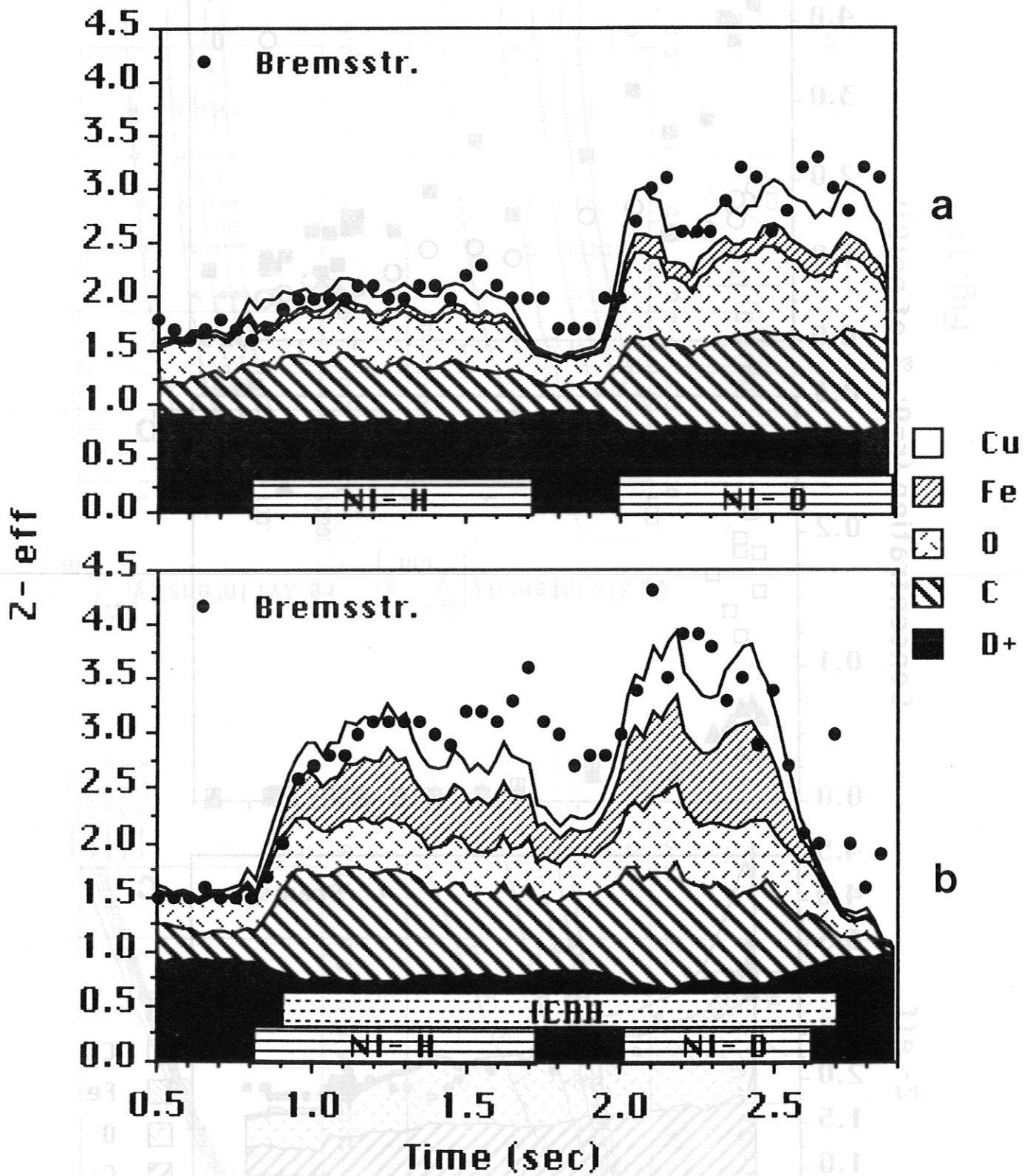


Fig. 12



IPP 3 JAN 24 - 89

Fig. 13

PROGRAM TO SOLVE THE IMPURITY TRANSPORT EQUATION FOR TOKAMAK TRANSPORT

FREE VARIABLE: TIME, RADIUS

INITIATION STATE

DENSITY- AND TEMPERATURE-PROFILES ARE CALCULATED FROM EXPERIMENTAL DATA OF VAX-DISTRIBUTION OR FROM NON-INTERFEROMETRY AND FOOT-DIAGNOSTICS OF THE PROGRAM. THE RESULTS ARE LISTED IN THE DATA FOR VENTURE ARE WRITTEN IN A ASCII FILE WHERE XXXX DENOTES A USER DEFINED NAME

Appendix A

PROFILES OF FAST NEUTRONS FROM NEUTRAL INJECTION ARE CALCULATED WITH THE CODE NEUMNT

Organization of ZEDIFF data files

THE ELEMENTS OF THE DATA FILES ARE DESCRIBED IN THE FOLLOWING

CHARACTER NAMES THE SECOND CHARACTER IS 'I' FOR INPUT AND 'O' FOR OUTPUT. FOR GARRON AND OXYGEN 'S' AS SECOND CHAR WITH SELECT RATE COEFFICIENTS FROM ITRAKA INSTEAD OF THE DATA FROM VAN REEMORTER

CALCULATIONS ARE PERFORMED WITH ANOMALOUS TRANSPORT AS WELL AS WITH NEOCCLASSICAL DIFFUSION. RUN THIS PROGRAM TO CREATE A PLASMA-DATABASE ON THE VAX WITH INPUT MENUES

TO START THE PROGRAM, ENTER 'ZEDIFF NAME TYPE MODE', WHERE - NAME IS STANDING FOR THE NAME AND - TYPE IS STANDING FOR THE TYPE AND - MODE IS STANDING FOR THE DISC MODE OF THE ACTUAL PLASMA-DATABASE

TWO FILES WHICH CONTAIN TIME-DEPENDENT DATA AND PROFILE DATA ARE SEND TO THE USERS READER LIST: - LINDAT CARDS - PRODAT CARDS

FOR THE VAX CLUSTER THERE ARE TWO ROUTINES AVAILABLE, TO READ THESE FILES IN THE IOL SYSTEM. THE DESTINATION OF THE PLOT METAFILE CAN BE SELECTED IN THE FILE 'ZEDIFF JOB' (READER LIST OR VARIOUS LASER PRINTERS)

PROGRAM TO SOLVE THE IMPURITY TRANSPORT EQUATION FOR TOKAMAK TRANSPORT

FREE VARIABLES : TIME, RADIUS
IONISATION STAGE

DENSITY- AND TEMPERATURE-PROFILES ARE CALCULATED FROM EXPERIMENTAL DATA OF YAG-DIFFRACTION OR FROM HCN-INTERFEROMETRY AND ECE-DIAGNOSTICS BY THE PROGRAM ZEDATA. THE RESULTING INPUT-DATA FOR ZEDIFF ARE WRITTEN IN A PLASMA DATAFILE 'FILE XXX' WHERE XXX MEANS A USER DEFINED NAME.

PROFILES OF FAST NEUTRALS (FROM NEUTRAL INJECTION) ARE CALCULATED WITH THE CODE ZENEUT.

THE ELEMENTSPECIFIC ATOMIC DATAFILES ARE NAMED 'XXDATEI', WHERE XX IS STANDING FOR THE CHEMICAL ELEMENT ABBREVIATION. FOR ONE-CHARACTER NAMES THE SECOND CHAR IS '1'.

FOR CARBON AND OXYGEN 2 AS SECOND CHAR WILL SELECT RATE COEFFICIENTS FROM ITIKAWA INSTEAD OF THE DATA FROM VAN REGEMORTER

CALCULATIONS ARE PERFORMED WITH ANOMALOUS TRANSPORT AS WELL AS WITH NEOCLASSICAL DIFFUSION.

ZEDATA

RUN THIS PROGRAM TO CREATE A PLASMA DATAFILE. ONLINE HELP WITH INPUT MENUES.

ZENEUT

TO START THE PROGRAM, ENTER 'ZENEUT NAME TYPE MODE', WHERE

- NAME IS STANDING FOR THE NAME AND
- TYPE IS STANDING FOR THE TYPE AND
- MODE IS STANDING FOR THE DISC MODE OF THE ACTUAL PLASMA DATAFILE

THE RESULTING OUTPUT FILE IS SEND TO THE USERS READER LIST WITH THE NAME 'PLADATA CARDS'

ZEDIFF

TO START THE PROGRAM, ENTER 'ZEDIFF NAME TYPE MODE', WHERE

- NAME IS STANDING FOR THE NAME AND
- TYPE IS STANDING FOR THE TYPE AND
- MODE IS STANDING FOR THE DISC MODE OF THE ACTUAL PLASMA DATAFILE

TWO FILES WHICH CONTAIN TIME DEPENDEND DATA AND PROFILE DATA ARE SEND TO THE USERS READER LIST:

- LINDAT CARDS
- PRODAT CARDS

FOR THE VAX CLUSTER THERE ARE TWO ROUTINES AVAILABLE, TO READ THESE FILES IN THE IDL SYSTEM.

THE DESTINATION OF THE PLOT METAFILE CAN BE SELECTED IN THE FILE 'ZEDIFF JCL' (READER LIST OR VARIOUS LASER PRINTERS).

PLASMA DATAFILE COMMENTS

DESCRIPTION OF HEADER

LINE 1 COL 1 : IMPURITY ELEMENTSIGN

2-5 : SPECTROSCOPIC LINES TO BE CALCULATED
 6 : LAST TIMEPOINT OF CALCULATION
 7 : SHOT-NUMBER
 LINE 2 1-5 : TIMEPOINTS FOR RADIAL PROFILES
 LINE 3 COL 1-2 : ANGLES FOR VIEW ON 3D PLOTS
 3-7 : RADIUS OF SIGHTLINES FOR 4 IONISATIONSTAGES AND
 SOFT X-RADIATION
 LINE 4,5 : 20 TIMEPOINTS FOR SAWTEETH
 6,7 : 20 TIMEPOINTS FOR BURSTS
 LINE 8 COL 1 : FLAG TO SIMULATE BLOW OFF EXPERIMENTS
 2 : NUMBER OF ABLATED PARTICLES
 3 : TIMEPOINT OF BLOW-OFF
 LINE 9 COL 1 : FLAG TO SIMULATE SINUSMODULATED GAS PUFFS
 2 : PARTICLE INFLUX PER CM CIRCUMFERENCE IN THE
 SINUS MAXIMA
 3 : BEGIN OF GASPUFF
 4 : END OF GASPUFF
 5 : MODULATION FREQUENCY
 LINE 10 COL 1 : FLAG FOR PLOT OF TRANSPORT COEFFICIENT PROFILES
 2 : FLAG FOR PLOT OF ION DENSITY, IMPURITY-CONCENTRATION
 AND ZEFF-PROFILES
 3 : FLAG FOR PLOT OF LINE RADIATION PROFILES
 4 : FLAG FOR PLOT OF TOTAL- AND SX-RADIATION PROFILES
 5 : FLAG FOR PLOT OF TIME EVOLUTION OF
 - PARTICLE LOSSES AND INFLUX
 - PARTICLE CONFINEMENT TIME
 6 : FLAG FOR PLOT OF TIME EVOLUTION OF
 - LINEINTEGRALS FOR SELECTED LINES AND SX-RADIATION
 - TOTAL RADIATION, IMPURITY CONCENTRATION AND ZEFF
 IN THE PLASMACENTER
 7 : FLAG FOR PLOT OF VARIOUS RADIAL PROFILES TO
 SELECTED TIMEPOINTS
 8 : FLAG FOR PLOT OF IMPURITY DENSITIES TO
 SELECTED TIMEPOINTS
 LINE 11 COL 1 : NI-INJECTION START TIME
 2 : NI-INJECTION END TIME
 3 : ICRH START TIME
 4 : ICRH END TIME
 LINE 12 COL 1 : MAJOR PLASMA RADIUS (CM)
 2 : MINOR PLASMA RADIUS (CM)
 3 : WIDTH OF SCRAPE-OFF LAYER (CM)
 4 : Q ON PLASMA EDGE
 5 : MAIN FIELD (TESLA)
 6 : PLASMA ION MASS (AMU)
 7 : BEAM ION MASS (AMU)
 8 : BEAM ENERGY (EV)
 LINE 13 COL 1 : GRID-TRANSFORMATION PARAMETER K; (RHO=R**K)
 2 : NUMBER OF GRID POINTS (MAXIMUM 128)
 3 : NUMBER OF DATASETS

DESCRIPTION OF DATASETS:

LINE 1 COLUMN 1 : NUMBER OF TIMESTEPS | COL1 * N ==> COL2 / N
 1 2 : TIMESTEP | COL2 / COL3 = DELTA-T
 1 3 : NUMBER OF ITERATION LOOPS | CHANGE ONLY BY EXPERTS
 1 4 : FACTOR OF DIELECTRONIC RECOMBINATION
 1 5 : FALL OFF LENGTH FOR NE PROFILES
 1 6 : FALL OFF LENGTH FOR TE PROFILES
 1 7 : NEUTRAL INJECTION POWER (W)
 1 8 : TIME-POINT

```

1      9 : SHAVRANOV SHIFT
2      1 : NEUTRAL FLUX FROM WALL (PART./(S*CM CIRCUMFERENCE))
2      2 : VELOCITY OF NEUTRAL IMPURITIES FROM WALL (CM/S)
2      3 : TAU SCRAPE-OFF - LIFETIME OF PARTICLES IN SCRAPE-OFF
          LAYER (S)
2      4 : TAU DIVERTOR - CONFINEMENT TIME OF PARTICLES IN
          DIVERTOR (S); ONLY VALID IF 2 6 # 0
2      5 : RECYCLING-COEFFICIENT OF WAND
2      6 : RECYCLING-COEFFICIENT OF DIVERTOR
3      1 : INNER DIFFUSION COEFFICIENT FOR ANOMALOUS TRANSPORT
          TAKE AS AN APPROACH D=4000 CM**2/S FOR OH-PHASE
          D=9000 CM**2/S FOR NI-PHASE
          D=0 => NEOCLASSICAL DIFFUSION ONLY
          D#0 => NEOCL. AND ANOMALOUS TRANSPORT
3      2 : OUTER DIFFUSION COEFFICIENT FOR ANOMALOUS TRANSPORT
          (DEFAULT: BOTH EQUAL)
3      3 : FACTOR FOR NEOCLASSICAL DIFFUSION
          =0 : WITHOUT NEOCL. DIFF.
          >0 : WITH NEOCL. DIFF. (EXACT NEOCL. WITH 1)
3      4 : FACTOR FOR INWARD-OUTWARD DRIFT
          DRIFT-VELOCITY ON EDGE = FACTOR*100 CM/S
          F=0 => NEOCLASSICAL DIFFUSION ONLY
          F#0 => NEOCL. AND ANOMALOUS TRANSPORT
3      5 : FLAG FOR FUNCTION V-INWARD(R)
          FLAG = 1 OR 2 : ANOMALOUS TRANSPORT
          TWO-STEP MODEL FOR DIFFUSION
          V-INWARD=FACTOR*(R/A)**FLAG (SEE 2 3)
          = 3 : NEOCLASSICAL TRANSPORT(SEE 2 2)
          +LINEAR ANOMALOUS TERM
          = 4 : NEOCLASSICAL TRANSPORT
          +QUADRATIC ANOMALOUS TERM
          = 5 OR 6 : ANOMALOUS TRANSPORT
          PARABOLIC MODEL FOR DIFFUSION
          V-INWARD=FACTOR*(R/A)**FLAG (SEE 2 3)
          = 7 : GENTLE/GEHRE TRANSPORT MODEL
          (CHANGES IN CODE REQUIRED, ONLY
          FOR SOPHISTICATED USERS)
3      6 : RADIUS OF CHANGE OF ANOMALOUS DIFFUSION COEFFICIENTS
3      7 : RADIUS OF SAWTEETH DIFFUSION BARRIER
3      8 : DISTANCE OF BURST DIFFUSION BARRIER FROM SEPARATRIX
4      1-4 : FITCOEFFICIENTS FOR ELECTRON TEMPERATURE
4      5 : FLAG FOR TE FIT
5      1-4 : FITCOEFFICIENTS FOR ELECTRON DENSITY
5      5 : FLAG FOR NE FIT
6,7, 1-4 : FITCOEFFICIENTS FOR NEUTRAL DENSITIES
8,9  5 : FLAG FOR NH FIT

```


'CU', 18, 19, 20, 24, 1.600, 27044
 5.000, 5.000, 5.000, 5.000, 5.000
 50, 30, 0.00, 0.00, 0.00, 0.00, 0.00, 0.00
 0.000, 0.000, 0.000, 0.000, 0.000, 0.000, 0.000, 0.000, 0.000, 0.000, 0.000, 0.000
 0.000, 0.000, 0.000, 0.000, 0.000, 0.000, 0.000, 0.000, 0.000, 0.000, 0.000, 0.000
 0.000, 0.000, 0.000, 0.000, 0.000, 0.000, 0.000, 0.000, 0.000, 0.000, 0.000, 0.000
 0.000, 0.000, 0.000, 0.000, 0.000, 0.000, 0.000, 0.000, 0.000, 0.000, 0.000, 0.000
 0, 0.00E+00, 0.000
 0, 0.00E+00, 0.000, 0.000, 0.000, 0.00
 1, 1, 1, 1, 1, 1, 1, 1, 1
 1.207, 1.589, 0.000, 0.000
 165.00, 40.00, 6.00, 3.00, 2.10, 2.00, 2.00, 40000.0
 1.0, 92, 30

100	0.1107E-01	20	0.50	2.00	2.00	0.00E+00	1.1073	0.039
0.100E+17	-0.230E+06	0.001	1.000	0.00	0.00			
6000.0	6000.0	0.000	-2.500	1	39.50	12.00	2.00	
6.8297E+00	-6.4081E+00	-6.773956E+01	4.748378E+01	2				
-8.0578E-01	-7.6220E+00	1.699577E+01	-2.812473E+02	2				
-2.5000E+01	0.0000E+00	0.000000E+00	0.000000E+00	3				
-2.5000E+01	0.0000E+00	0.000000E+00	0.000000E+00	3				
-2.5000E+01	0.0000E+00	0.000000E+00	0.000000E+00	3				
-3.9980E+00	4.3643E+01	-2.309000E+00	-3.696189E+02	3				

20	0.8300E-03	20	0.50	2.00	2.00	0.00E+00	1.1239	0.039
0.100E+17	-0.230E+06	0.001	1.000	0.00	0.00			
6000.0	6000.0	1.000	0.000	3	39.5	12.00	2.00	
6.7928E+00	-5.3757E+00	-7.536035E+01	2.946211E+01	2				
-8.3781E-01	-6.5899E+00	1.526318E+01	-2.721829E+02	2				
-2.5000E+01	0.0000E+00	0.000000E+00	0.000000E+00	3				
-2.5000E+01	0.0000E+00	0.000000E+00	0.000000E+00	3				
-2.5000E+01	0.0000E+00	0.000000E+00	0.000000E+00	3				
-3.9980E+00	4.3643E+01	-2.309000E+00	-3.696189E+02	3				

20	0.8300E-03	20	0.50	2.00	2.00	0.00E+00	1.1405	0.039
0.100E+17	-0.230E+06	0.001	1.000	0.00	0.00			
6000.0	6000.0	1.000	0.000	3	39.5	12.00	2.00	
6.6675E+00	-7.9738E-01	-1.165179E+02	1.327322E+02	2				
-8.8450E-01	-4.2327E+00	-9.269588E+00	-2.250305E+02	2				
-2.5000E+01	0.0000E+00	0.000000E+00	0.000000E+00	3				
-2.5000E+01	0.0000E+00	0.000000E+00	0.000000E+00	3				
-2.5000E+01	0.0000E+00	0.000000E+00	0.000000E+00	3				
-3.9980E+00	4.3643E+01	-2.309000E+00	-3.696189E+02	3				

20	0.8300E-03	20	0.50	2.00	2.00	0.00E+00	1.1571	0.039
0.100E+17	-0.230E+06	0.001	1.000	0.00	0.00			
6000.0	6000.0	1.000	0.000	3	39.5	12.00	2.00	
6.6195E+00	2.7544E-01	-1.258501E+02	1.548494E+02	2				
-8.6969E-01	-4.2874E+00	-6.839355E+00	-2.517095E+02	2				
-2.5000E+01	0.0000E+00	0.000000E+00	0.000000E+00	3				
-2.5000E+01	0.0000E+00	0.000000E+00	0.000000E+00	3				
-2.5000E+01	0.0000E+00	0.000000E+00	0.000000E+00	3				
-3.9980E+00	4.3643E+01	-2.309000E+00	-3.696189E+02	3				

20	0.8300E-03	20	0.50	2.00	2.00	0.00E+00	1.1738	0.039
0.100E+17	-0.230E+06	0.001	1.000	0.00	0.00			
6000.0	6000.0	1.000	0.000	3	39.5	12.00	2.00	
6.6528E+00	-2.8605E+00	-9.163495E+01	5.264767E+01	2				
-8.3059E-01	-4.9005E+00	6.846539E+00	-2.972578E+02	2				
-2.5000E+01	0.0000E+00	0.000000E+00	0.000000E+00	3				
-2.5000E+01	0.0000E+00	0.000000E+00	0.000000E+00	3				
-2.5000E+01	0.0000E+00	0.000000E+00	0.000000E+00	3				
-3.9980E+00	4.3643E+01	-2.309000E+00	-3.696189E+02	3				

20	0.8300E-03	20	0.50	2.00	2.00	0.00E+00	1.1904	0.039
0.100E+17	-0.230E+06	0.001	1.000	0.00	0.00			
6000.0	6000.0	1.000	0.000	3	39.5	12.00	2.00	
6.7163E+00	-6.3695E+00	-4.864561E+01	-1.895561E+01	2				
-8.0860E-01	-4.2673E+00	-1.081846E+00	-2.853162E+02	2				
-2.5000E+01	0.0000E+00	0.000000E+00	0.000000E+00	3				

-2.5000E+01	0.0000E+00	0.000000E+00	0.000000E+00	3				
-2.5000E+01	0.0000E+00	0.000000E+00	0.000000E+00	3				
-3.9980E+00	4.3643E+01	-2.309000E+00	-3.696189E+02	3				
20	0.8300E-03	20	0.50	2.00	2.00	0.21E+07	1.2070	0.050
0.500E+17	-0.230E+06	0.001	1.000	0.00	0.00			
10000.0	10000.0	1.000	0.000	3	39.5	12.00	2.00	
6.9053E+00	-1.0617E+01	5.104820E+00	-1.274177E+02	2				
-7.5844E-01	-4.5880E+00	-9.022713E-01	-2.911257E+02	2				
-2.5000E+01	0.0000E+00	0.000000E+00	0.000000E+00	3				
-2.5000E+01	0.0000E+00	0.000000E+00	0.000000E+00	3				
-2.5000E+01	0.0000E+00	0.000000E+00	0.000000E+00	3				
-3.9980E+00	4.3643E+01	-2.309000E+00	-3.696189E+02	3				
20	0.8300E-03	20	0.50	2.00	2.00	0.21E+07	1.2237	0.061
0.500E+17	-0.230E+06	0.001	1.000	0.00	0.00			
10000.0	10000.0	1.000	0.000	3	39.5	12.00	2.00	
7.1410E+00	-1.3551E+01	6.159366E+01	-3.957192E+02	2				
-6.9551E-01	-6.8168E+00	2.626123E+01	-3.627725E+02	2				
-2.5000E+01	0.0000E+00	0.000000E+00	0.000000E+00	3				
-2.5000E+01	0.0000E+00	0.000000E+00	0.000000E+00	3				
-2.5000E+01	0.0000E+00	0.000000E+00	0.000000E+00	3				
-3.9980E+00	4.3643E+01	-2.309000E+00	-3.696189E+02	3				
20	0.8300E-03	20	0.50	2.00	2.00	0.21E+07	1.2403	0.065
0.500E+17	-0.230E+06	0.001	1.000	0.00	0.00			
10000.0	10000.0	1.000	0.000	3	39.5	12.00	2.00	
7.2509E+00	-1.4011E+01	9.782355E+01	-5.942830E+02	2				
-6.4290E-01	-1.0118E+01	6.115607E+01	-4.587178E+02	2				
-2.5000E+01	0.0000E+00	0.000000E+00	0.000000E+00	3				
-2.5000E+01	0.0000E+00	0.000000E+00	0.000000E+00	3				
-2.5000E+01	0.0000E+00	0.000000E+00	0.000000E+00	3				
-3.9980E+00	4.3643E+01	-2.309000E+00	-3.696189E+02	3				
20	0.8300E-03	20	0.50	2.00	2.00	0.21E+07	1.2569	0.067
0.500E+17	-0.230E+06	0.001	1.000	0.00	0.00			
10000.0	10000.0	1.000	0.000	3	39.5	12.00	2.00	
7.3074E+00	-1.4127E+01	1.024027E+02	-5.900786E+02	2				
-5.8944E-01	-1.3856E+01	9.072888E+01	-5.279312E+02	2				
-2.5000E+01	0.0000E+00	0.000000E+00	0.000000E+00	3				
-2.5000E+01	0.0000E+00	0.000000E+00	0.000000E+00	3				
-2.5000E+01	0.0000E+00	0.000000E+00	0.000000E+00	3				
-3.9980E+00	4.3643E+01	-2.309000E+00	-3.696189E+02	3				
20	0.8300E-03	20	0.50	2.00	2.00	0.21E+07	1.2735	0.067
0.500E+17	-0.230E+06	0.001	1.000	0.00	0.00			
10000.0	10000.0	1.000	0.000	3	39.5	12.00	2.00	
7.3852E+00	-1.4588E+01	1.057700E+02	-6.092610E+02	2				
-5.4906E-01	-1.7714E+01	1.289004E+02	-6.243982E+02	2				
-2.5000E+01	0.0000E+00	0.000000E+00	0.000000E+00	3				
-2.5000E+01	0.0000E+00	0.000000E+00	0.000000E+00	3				
-2.5000E+01	0.0000E+00	0.000000E+00	0.000000E+00	3				
-3.9980E+00	4.3643E+01	-2.309000E+00	-3.696189E+02	3				
20	0.8300E-03	20	0.50	2.00	2.00	0.21E+07	1.2902	0.067
0.500E+17	-0.230E+06	0.001	1.000	0.00	0.00			
10000.0	10000.0	1.000	0.000	3	39.5	12.00	2.00	
7.3841E+00	-1.3169E+01	1.073199E+02	-6.654119E+02	2				
-6.3348E-01	-1.6636E+01	1.325903E+02	-6.627798E+02	2				
-2.5000E+01	0.0000E+00	0.000000E+00	0.000000E+00	3				
-2.5000E+01	0.0000E+00	0.000000E+00	0.000000E+00	3				
-2.5000E+01	0.0000E+00	0.000000E+00	0.000000E+00	3				
-3.9980E+00	4.3643E+01	-2.309000E+00	-3.696189E+02	3				
20	0.8300E-03	20	0.50	2.00	2.00	0.21E+07	1.3068	0.068
0.500E+17	-0.230E+06	0.001	1.000	0.00	0.00			
10000.0	10000.0	1.000	0.000	3	39.5	12.00	2.00	
7.3406E+00	-1.1294E+01	1.025844E+02	-6.948660E+02	2				
-7.7132E-01	-1.2562E+01	1.252725E+02	-7.107551E+02	2				
-2.5000E+01	0.0000E+00	0.000000E+00	0.000000E+00	3				

-2.5000E+01	0.0000E+00	0.000000E+00	0.000000E+00	3				
-2.5000E+01	0.0000E+00	0.000000E+00	0.000000E+00	3				
-3.9980E+00	4.3643E+01	-2.309000E+00	-3.696189E+02	3				
20	0.8300E-03	20	0.50	2.00	2.00	0.21E+07	1.3234	0.074
0.500E+17	-0.230E+06	0.001	1.000	0.00	0.00			
3000.0	10000.0	1.000	0.000	3	39.5	12.00	2.00	
7.3804E+00	-1.3043E+01	1.316339E+02	-8.053191E+02	2				
-7.7806E-01	-1.1747E+01	1.622789E+02	-8.934995E+02	2				
-2.5000E+01	0.0000E+00	0.000000E+00	0.000000E+00	3				
-2.5000E+01	0.0000E+00	0.000000E+00	0.000000E+00	3				
-2.5000E+01	0.0000E+00	0.000000E+00	0.000000E+00	3				
-3.9980E+00	4.3643E+01	-2.309000E+00	-3.696189E+02	3				
20	0.8300E-03	20	0.50	2.00	2.00	0.21E+07	1.3400	0.076
0.500E+17	-0.230E+06	0.001	1.000	0.00	0.00			
3000.0	10000.0	1.000	0.000	3	39.5	12.00	2.00	
7.3995E+00	-1.4223E+01	1.452703E+02	-8.318616E+02	2				
-7.0899E-01	-1.1099E+01	1.760812E+02	-9.710278E+02	2				
-2.5000E+01	0.0000E+00	0.000000E+00	0.000000E+00	3				
-2.5000E+01	0.0000E+00	0.000000E+00	0.000000E+00	3				
-2.5000E+01	0.0000E+00	0.000000E+00	0.000000E+00	3				
-3.9980E+00	4.3643E+01	-2.309000E+00	-3.696189E+02	3				
20	0.8300E-03	20	0.50	2.00	2.00	0.21E+07	1.3567	0.077
0.500E+17	-0.230E+06	0.001	1.000	0.00	0.00			
3000.0	10000.0	1.000	0.000	3	39.5	12.00	2.00	
7.3776E+00	-1.4968E+01	1.252910E+02	-7.006045E+02	2				
-6.0184E-01	-1.1190E+01	1.357703E+02	-7.892725E+02	2				
-2.5000E+01	0.0000E+00	0.000000E+00	0.000000E+00	3				
-2.5000E+01	0.0000E+00	0.000000E+00	0.000000E+00	3				
-2.5000E+01	0.0000E+00	0.000000E+00	0.000000E+00	3				
-3.9980E+00	4.3643E+01	-2.309000E+00	-3.696189E+02	3				
20	0.8300E-03	20	0.50	2.00	2.00	0.21E+07	1.3733	0.066
0.500E+17	-0.230E+06	0.001	1.000	0.00	0.00			
3000.0	10000.0	1.000	0.000	3	39.5	12.00	2.00	
7.3650E+00	-1.6368E+01	1.068621E+02	-5.782173E+02	2				
-5.0667E-01	-1.5313E+01	1.059920E+02	-5.710459E+02	2				
-2.5000E+01	0.0000E+00	0.000000E+00	0.000000E+00	3				
-2.5000E+01	0.0000E+00	0.000000E+00	0.000000E+00	3				
-2.5000E+01	0.0000E+00	0.000000E+00	0.000000E+00	3				
-3.9980E+00	4.3643E+01	-2.309000E+00	-3.696189E+02	3				
20	0.8300E-03	20	0.50	2.00	2.00	0.21E+07	1.3899	0.062
0.500E+17	-0.230E+06	0.001	1.000	0.00	0.00			
3000.0	10000.0	1.000	0.000	3	39.5	12.00	2.00	
7.2884E+00	-1.2329E+01	5.740805E+01	-4.304780E+02	2				
-4.8384E-01	-2.1993E+01	1.500151E+02	-6.379102E+02	2				
-2.5000E+01	0.0000E+00	0.000000E+00	0.000000E+00	3				
-2.5000E+01	0.0000E+00	0.000000E+00	0.000000E+00	3				
-2.5000E+01	0.0000E+00	0.000000E+00	0.000000E+00	3				
-3.9980E+00	4.3643E+01	-2.309000E+00	-3.696189E+02	3				
20	0.8300E-03	20	0.50	2.00	2.00	0.21E+07	1.4066	0.062
0.500E+17	-0.230E+06	0.001	1.000	0.00	0.00			
3000.0	10000.0	1.000	0.000	3	39.5	12.00	2.00	
7.2260E+00	-7.8602E+00	1.656168E+01	-3.371721E+02	2				
-4.7956E-01	-2.6786E+01	2.115740E+02	-8.248513E+02	2				
-2.5000E+01	0.0000E+00	0.000000E+00	0.000000E+00	3				
-2.5000E+01	0.0000E+00	0.000000E+00	0.000000E+00	3				
-2.5000E+01	0.0000E+00	0.000000E+00	0.000000E+00	3				
-3.9980E+00	4.3643E+01	-2.309000E+00	-3.696189E+02	3				
20	0.8300E-03	20	0.50	2.00	2.00	0.21E+07	1.4232	0.062
0.500E+17	-0.230E+06	0.001	1.000	0.00	0.00			
3000.0	10000.0	1.000	0.000	3	39.5	12.00	2.00	
7.2362E+00	-8.2365E+00	2.135355E+01	-3.551216E+02	2				
-6.0894E-01	-2.4363E+01	2.012443E+02	-8.196897E+02	2				
-2.5000E+01	0.0000E+00	0.000000E+00	0.000000E+00	3				

-2.5000E+01	0.0000E+00	0.000000E+00	0.000000E+00	3				
-2.5000E+01	0.0000E+00	0.000000E+00	0.000000E+00	3				
-3.9980E+00	4.3643E+01	-2.309000E+00	-3.696189E+02	3				
20	0.8300E-03	20	0.50	2.00	2.00	0.21E+07	1.4398	0.061
0.500E+17	-0.230E+06	0.001	1.000	0.00	0.00			
3000.0	10000.0	1.000	0.000	3	39.5	12.00	2.00	
7.2840E+00	-1.0947E+01	4.687363E+01	-4.183962E+02	2				
-7.4826E-01	-2.1259E+01	1.813907E+02	-7.873777E+02	2				
-2.5000E+01	0.0000E+00	0.000000E+00	0.000000E+00	3				
-2.5000E+01	0.0000E+00	0.000000E+00	0.000000E+00	3				
-2.5000E+01	0.0000E+00	0.000000E+00	0.000000E+00	3				
-3.9980E+00	4.3643E+01	-2.309000E+00	-3.696189E+02	3				
20	0.8300E-03	20	0.50	2.00	2.00	0.21E+07	1.4564	0.061
0.500E+17	-0.230E+06	0.001	1.000	0.00	0.00			
3000.0	10000.0	1.000	0.000	3	39.5	12.00	2.00	
7.3485E+00	-1.3509E+01	7.127057E+01	-4.801648E+02	2				
-6.8056E-01	-2.3697E+01	2.137520E+02	-8.971521E+02	2				
-2.5000E+01	0.0000E+00	0.000000E+00	0.000000E+00	3				
-2.5000E+01	0.0000E+00	0.000000E+00	0.000000E+00	3				
-2.5000E+01	0.0000E+00	0.000000E+00	0.000000E+00	3				
-3.9980E+00	4.3643E+01	-2.309000E+00	-3.696189E+02	3				
20	0.8300E-03	20	0.50	2.00	2.00	0.21E+07	1.4731	0.062
0.500E+17	-0.230E+06	0.001	1.000	0.00	0.00			
3000.0	10000.0	1.000	0.000	3	39.5	12.00	2.00	
7.3785E+00	-1.4099E+01	7.777673E+01	-4.973367E+02	2				
-6.1942E-01	-2.4732E+01	2.349313E+02	-9.791082E+02	2				
-2.5000E+01	0.0000E+00	0.000000E+00	0.000000E+00	3				
-2.5000E+01	0.0000E+00	0.000000E+00	0.000000E+00	3				
-2.5000E+01	0.0000E+00	0.000000E+00	0.000000E+00	3				
-3.9980E+00	4.3643E+01	-2.309000E+00	-3.696189E+02	3				
20	0.8300E-03	20	0.50	2.00	2.00	0.21E+07	1.4897	0.063
0.500E+17	-0.230E+06	0.001	1.000	0.00	0.00			
3000.0	10000.0	1.000	0.000	3	39.5	12.00	2.00	
7.3820E+00	-1.4294E+01	8.679614E+01	-5.474207E+02	2				
-6.9922E-01	-2.0622E+01	2.004264E+02	-8.927524E+02	2				
-2.5000E+01	0.0000E+00	0.000000E+00	0.000000E+00	3				
-2.5000E+01	0.0000E+00	0.000000E+00	0.000000E+00	3				
-2.5000E+01	0.0000E+00	0.000000E+00	0.000000E+00	3				
-3.9980E+00	4.3643E+01	-2.309000E+00	-3.696189E+02	3				
20	0.8300E-03	20	0.50	2.00	2.00	0.21E+07	1.5063	0.064
0.500E+17	-0.230E+06	0.001	1.000	0.00	0.00			
3000.0	10000.0	1.000	0.000	3	39.5	12.00	2.00	
7.3689E+00	-1.3550E+01	8.297156E+01	-5.536304E+02	2				
-8.1898E-01	-1.4965E+01	1.477437E+02	-7.551196E+02	2				
-2.5000E+01	0.0000E+00	0.000000E+00	0.000000E+00	3				
-2.5000E+01	0.0000E+00	0.000000E+00	0.000000E+00	3				
-2.5000E+01	0.0000E+00	0.000000E+00	0.000000E+00	3				
-3.9980E+00	4.3643E+01	-2.309000E+00	-3.696189E+02	3				
20	0.8300E-03	20	0.50	2.00	2.00	0.21E+07	1.5230	0.065
0.500E+17	-0.230E+06	0.001	1.000	0.00	0.00			
3000.0	10000.0	1.000	0.000	3	39.5	12.00	2.00	
7.3638E+00	-1.3256E+01	7.754126E+01	-5.105903E+02	2				
-8.4479E-01	-1.2121E+01	1.250539E+02	-7.180342E+02	2				
-2.5000E+01	0.0000E+00	0.000000E+00	0.000000E+00	3				
-2.5000E+01	0.0000E+00	0.000000E+00	0.000000E+00	3				
-2.5000E+01	0.0000E+00	0.000000E+00	0.000000E+00	3				
-3.9980E+00	4.3643E+01	-2.309000E+00	-3.696189E+02	3				
20	0.8300E-03	20	0.50	2.00	2.00	0.21E+07	1.5396	0.065
0.500E+17	-0.230E+06	0.001	1.000	0.00	0.00			
3000.0	10000.0	1.000	0.000	3	39.5	12.00	2.00	
7.4027E+00	-1.5358E+01	8.963000E+01	-5.033435E+02	2				
-8.0947E-01	-1.1335E+01	1.164355E+02	-6.973428E+02	2				
-2.5000E+01	0.0000E+00	0.000000E+00	0.000000E+00	3				

-2.5000E+01	0.0000E+00	0.000000E+00	0.000000E+00	3
-2.5000E+01	0.0000E+00	0.000000E+00	0.000000E+00	3
-3.9980E+00	4.3643E+01	-2.309000E+00	-3.696189E+02	3

20	0.8300E-03	20	0.50	2.00	2.00	0.21E+07	1.5562	0.067
0.500E+17	-0.230E+06	0.001	1.000	0.00	0.00			
3000.0	10000.0	1.000	0.000	3	39.5	12.00	2.00	
7.4404E+00	-1.6347E+01	9.259698E+01	-5.055847E+02	2				
-7.9135E-01	-1.1812E+01	1.215425E+02	-7.011953E+02	2				
-2.5000E+01	0.0000E+00	0.000000E+00	0.000000E+00	3				
-2.5000E+01	0.0000E+00	0.000000E+00	0.000000E+00	3				
-2.5000E+01	0.0000E+00	0.000000E+00	0.000000E+00	3				
-3.9980E+00	4.3643E+01	-2.309000E+00	-3.696189E+02	3				

20	0.8300E-03	20	0.50	2.00	2.00	0.21E+07	1.5728	0.067
0.500E+17	-0.230E+06	0.001	1.000	0.00	0.00			
3000.0	10000.0	1.000	0.000	3	39.5	12.00	2.00	
7.4356E+00	-1.6138E+01	1.100012E+02	-5.974690E+02	2				
-7.5024E-01	-1.3967E+01	1.673505E+02	-8.696738E+02	2				
-2.5000E+01	0.0000E+00	0.000000E+00	0.000000E+00	3				
-2.5000E+01	0.0000E+00	0.000000E+00	0.000000E+00	3				
-2.5000E+01	0.0000E+00	0.000000E+00	0.000000E+00	3				
-3.9980E+00	4.3643E+01	-2.309000E+00	-3.696189E+02	3				

20	0.8300E-03	20	0.50	2.00	2.00	0.21E+07	1.5895	0.070
0.500E+17	-0.230E+06	0.001	1.000	0.00	0.00			
3000.0	10000.0	1.000	0.000	3	39.5	12.00	2.00	
7.3628E+00	-1.4000E+01	1.107069E+02	-6.457388E+02	2				
-7.2178E-01	-1.3237E+01	1.873829E+02	-9.723555E+02	2				
-2.5000E+01	0.0000E+00	0.000000E+00	0.000000E+00	3				
-2.5000E+01	0.0000E+00	0.000000E+00	0.000000E+00	3				
-2.5000E+01	0.0000E+00	0.000000E+00	0.000000E+00	3				
-3.9980E+00	4.3643E+01	-2.309000E+00	-3.696189E+02	3				

[Faint, mostly illegible text and data blocks, likely bleed-through from the reverse side of the page.]

ATOM DATA FILE COMMENTS

THE DATA ARE TAKEN FROM ABELS-VAN MAANEN, J. J. (1971) 77
THE MOMENTS AT THE END OF THE LINE ARE IN THIS REPORT

THE STRONGEST LINE OF THIS IONISATION STAGE
IS THE STRONGEST LINE OF THIS IONISATION STAGE

List of atomic data files for elements:

Appendix B

H, He, Be, B, C, O, Ne, Al, Si, S, Cl, Ar, Ti, Cr, Fe, Ni, Cu

Atomic data files used in ZEDIFF

Element	Ionisation Stage	File Name
H	1	1.1.LINE
He	1	2.1.LINE
Be	1	3.1.LINE
B	1	4.1.LINE
C	1	5.1.LINE
O	1	6.1.LINE
Ne	1	7.1.LINE
Al	1	8.1.LINE
Si	1	9.1.LINE
S	1	10.1.LINE
Cl	1	11.1.LINE
Ar	1	12.1.LINE
Ti	1	13.1.LINE
Cr	1	14.1.LINE
Fe	1	15.1.LINE
Ni	1	16.1.LINE
Cu	1	17.1.LINE

-2.5000E+01	0.0000E+00	0.000000E+00	0.500000E+00	3
-2.5000E+01	0.0000E+00	0.000000E+00	0.000000E+00	3
-3.9980E+00	4.3643E+01	-2.308000E+00	-3.595189E+02	3

List of atomic data files for elements:

H, He, Be, B, C, O, Ne, Al, Si, S, Cl, Ar, Ti, Cr, Fe, Ni, Cu

0.5000E+17	-0.2300E+05	0.001	1.000	0.00	0.00
3000.0	10000.0	1.000	0.000	3	38.5
7.4255E+00	-1.8130E+01	1.107069E+02	-4.657388E+02	2	
-7.2178E-01	-1.3237E+01	1.673829E+02	-9.723555E+02	2	
-2.5000E+01	0.0000E+00	0.000000E+00	0.000000E+00	3	
-2.5000E+01	0.0000E+00	0.000000E+00	0.000000E+00	3	
-2.5000E+01	0.0000E+00	0.000000E+00	0.000000E+00	3	
-3.9980E+00	4.3643E+01	-2.308000E+00	-3.595189E+02	3	

20	0.8300E-03	20	0.50	2.00	2.00	0.216+07	1.5685	0.067
0.5000E+17	-0.2300E+05	0.001	1.000	0.00	0.00			
3000.0	10000.0	1.000	0.000	3	38.5	12.00	2.00	
7.4255E+00	-1.8130E+01	1.107069E+02	-4.657388E+02	2				
-7.2178E-01	-1.3237E+01	1.673829E+02	-9.723555E+02	2				
-2.5000E+01	0.0000E+00	0.000000E+00	0.000000E+00	3				
-2.5000E+01	0.0000E+00	0.000000E+00	0.000000E+00	3				
-2.5000E+01	0.0000E+00	0.000000E+00	0.000000E+00	3				
-3.9980E+00	4.3643E+01	-2.308000E+00	-3.595189E+02	3				

ATOM DATAFILE COMMENTS

THE DATA ARE TAKEN FROM ABELS-VAN MAANEN, JET-DN-T (85) 27

THE COMMENTS AT THE END OF THE LINES BASE ON THIS REPORT

28

LINE 1 COL 1 : IONISATIONSTAGE
2 : WAVELENGTH OF 1. LINE (A) - SHOULD BE THE STRONGEST
LINE OF THIS IONISATIONSTAGE
3 : ENERGY OF 1. LINE (EV) DE 1.LINE
4 : EFFECTIVE ENERGY OF 1. LINE
- ABOUT VALUE OF 3 IF ALL OTHER LINES ARE WEAK
- > VALUE OF 3 IF OTHER STRONG LINES EXIST
5 : OSCILLATOR STRENGTH OF 1. LINE F 1.LINE
6 : GAUNT FACTOR 1. LINE G 1.LINE
7 : ENERGY OF 1. LINE (EV) DE 2.LINE

8 : OSCILLATOR STRENGTH OF 1. LINE F 2.LINE
9 : GAUNT FACTOR 1. LINE G 2.LINE

SET 7-9 ZERO IF THERE EXIST ONLY DATA FOR ONE LINE
SET 6,9 NEGATIVE IF ITS A DELTA N = 1 LINE

LINE 2 COL 1 : LOTZ-COEFFICIENTS A 1.LINE
2 : A 2.LINE
3 : B 1.LINE
4 : B 2.LINE
5 : C 1.LINE
6 : C 2.LINE
7 : P 1.LINE
8 : P 2.LINE
9 : Q 1.LINE
10 : Q 2.LINE
11 : MAIN QUANTUM NUMBER WAVELENGTH TABLE
12 : NUMBER OF ELECTRONS OF RECOMBINING ION

THE DATA ARE TAKEN FROM ABELS-VAN MAANEN, JET-DN-7 (85) 27

HADES* GUJ:ATODAT.H1DATEI 24.11.89 10:23:33 PAGE 1

LINE 1 COL 1 : IONISATIONSTAGE
 2 : WAVELENGTH OF 1. LINE
 3 : WAVELENGTH OF 2. LINE
 4 : EFFECTIVE ENERGY OF 1. LINE
 5 : EFFECTIVE ENERGY OF 2. LINE
 6 : ABOUT VALUE OF 3 IF ALL OTHER LINES ARE WEAK
 7 : OSCILLATOR STRENGTH OF 1. LINE
 8 : OSCILLATOR STRENGTH OF 2. LINE
 9 : GAUNT FACTOR 1. LINE
 10 : GAUNT FACTOR 2. LINE
 11 : ENERGY OF 1. LINE (eV)
 12 : ENERGY OF 2. LINE (eV)

1,	1215.0,	10.0,	0.42,	0.80																
		10.0,	0.42,	0.80,	12.0,	0.08,	0.80													
4.0,	0.	0.60,	0.	0.56,	0.	13.6,	13.6,	1.0,	0.	1.	0.									

elements:
 H, He, Li, Be, B, C, N, O, Ne, Ar, Si, S, Cl, Ar, Ti, Cr, Fe, Ni, Cu

SET 7-9 ZERO IF THERE EXIST ONLY DATA FOR ONE LINE
 SET 8,9 NEGATIVE IF ITS A BETA N + 1 LINE

LINE 2 COL 1 : COEFFICIENTS
 2 :
 3 :
 4 :
 5 :
 6 :
 7 :
 8 :
 9 :
 10 :
 11 : MAIN QUANTUM NUMBER
 12 : NUMBER OF ELECTRONS OF RECOMBINING ION

1,	2348.0,	5.3,	1.36,	1.00	0.0,	0.0,	1.00		
4.0,	4.4,	0.70,	0.60,	0.50,	0.60,	9.3,	115.0,	2.0,	2.0,
2,	3130.6,	4.0,	0.50,	0.25					
4.4,	4.5,	0.0,	0.40,	0.0,	0.60,	11.9,	0.08,	0.25	
3,	100.3,	123.6,	0.55,	-0.30		18.2,	125.0,	1.0,	2.0,
4.5,	0.0,	0.30,	0.0,	0.60,	0.0,	140.0,	0.13,	-0.25	
4,	77.5,	160.0,	0.42,	-0.25		154.0,	154.0,	2.0,	0.0,
4.5,	0.0,	0.0,	0.0,	0.0,	0.0,	193.0,	0.07,	-0.25	
		200.0,	0.42,	-0.25,		218.0,	218.0,	1.0,	0.0,

1,	735.9,	16.8,	0.17,	0.25	0.0,	0.0,	0.0			
2.6,	4.0,	0.92,	0.70,	0.19,	0.50,	21.6,	48.5,	6.0,	2.0,	2., 7.
2,	460.7,	26.9,	0.33,	0.80	0.0,	0.0,	0.0			
3.2,	4.4,	0.83,	0.40,	0.48,	0.60,	41.1,	66.4,	5.0,	2.0,	2., 6.
3,	488.1,	25.4,	0.26,	0.80	50.0,	0.71,	-0.25			
4.2,	4.5,	0.50,	0.20,	0.60,	0.60,	63.5,	86.2,	4.0,	2.0,	2., 5.
4,	542.8,	22.8,	0.34,	0.80	62.0,	0.60,	-0.25			
4.5,	4.5,	0.20,	0.0,	0.60,	0.0,	97.1,	108.0,	3.0,	2.0,	2., 4.
5,	568.4,	26.0,	0.40,	0.80	87.0,	0.82,	-0.25			
4.5,	4.5,	0.0,	0.0,	0.0,	0.0,	126.0,	139.0,	2.0,	2.0,	2., 3.
6,	558.6,	27.5,	0.43,	0.80	101.0,	0.56,	-0.25			
4.5,	4.5,	0.0,	0.0,	0.0,	0.0,	158.0,	172.0,	1.0,	2.0,	2., 2.
7,	465.2,	24.8,	0.43,	0.80	127.0,	0.50,	-0.25			
4.5,	4.5,	0.0,	0.0,	0.0,	0.0,	207.0,	1073.0,	2.0,	2.0,	2., 1.
8,	773.7,	16.0,	0.15,	0.80	141.0,	1.00,	-0.25			
4.5,	4.5,	0.0,	0.0,	0.0,	0.0,	239.0,	1107.0,	1.0,	2.0,	2., 0.
9,	11.6,	1072.0,	0.15,	-0.25	921.0,	0.72,	-1.00			
4.5,	4.5,	0.0,	0.0,	0.0,	0.0,	1196.0,	1196.0,	2.0,	0.0,	1., 1.
10,	12.1,	1022.0,	0.42,	-0.50	1211.0,	0.08,	-0.25			
4.5,	4.5,	0.0,	0.0,	0.0,	0.0,	1362.0,	1362.0,	1.0,	0.0,	1., 0.

1,	1687.5,	10.1,	0.12,	1.00					
		9.5,	0.12,	1.00,	8.6,	0.24,	-1.00		
4.0,	4.0,	0.40,	0.60,	0.60,	10.4,	20.2,	4.0,	2.0,	3., 5.
2,	1253.8,	9.9,	0.01,	0.20					
		16.2,	0.01,	0.20,	14.1,	0.06,	-0.20		
4.4,	4.4,	0.30,	0.20,	0.60,	23.4,	30.7,	3.0,	2.0,	3., 4.
3,	1201.0,	10.4,	0.51,	0.20					
		17.9,	0.51,	0.20,	21.1,	0.47,	0.20		
4.5,	4.5,	0.,	0.,	0.,	35.0,	43.8,	2.0,	2.0,	3., 3.
4,	1062.7,	11.7,	0.59,	0.20					
		17.1,	0.59,	0.20,	22.5,	0.09,	-0.20		
4.5,	4.5,	0.,	0.,	0.60,	47.3,	57.6,	1.0,	2.0,	3., 2.
5,	786.5,	15.8,	1.46,	0.20					
		27.2,	1.46,	0.20,	38.6,	0.10,	-0.25		
4.5,	4.5,	0.,	0.,	0.,	72.7,	239.0,	2.0,	6.0,	3., 1.
6,	933.4,	13.3,	0.43,	0.25					
		42.8,	0.43,	0.25,	45.0,	0.09,	-0.25		
4.5,	4.5,	0.,	0.,	0.,	88.1,	257.0,	1.0,	6.0,	3., 0.
7,	72.0,	172.1,	0.20,	-0.20					
		220.1,	0.20,	-0.20,	206.0,	1.54,	-0.25		
4.5,	4.5,	0.,	0.,	0.,	281.0,	343.0,	6.0,	2.0,	2., 7.
8,	198.6,	62.4,	0.10,	0.20					
		205.2,	0.10,	0.20,	195.2,	0.18,	-0.25		
4.5,	4.5,	0.,	0.,	0.,	328.0,	384.0,	5.0,	2.0,	2., 6.
9,	54.2,	228.9,	0.06,	-0.25					
		271.3,	0.06,	-0.25,	234.6,	0.02,	-0.25		
4.5,	4.5,	0.,	0.,	0.,	379.0,	426.0,	4.0,	2.0,	2., 5.
10,	49.3,	261.9,	0.03,	-0.25					
		297.8,	0.03,	-0.25,	262.8,	0.03,	-0.25		
4.5,	4.5,	0.,	0.,	0.,	447.0,	469.0,	3.0,	2.0,	2., 4.
11,	189.9,	66.3,	0.08,	0.25					
		233.7,	0.08,	0.25,	44.0,	0.06,	0.25		
4.5,	4.5,	0.,	0.,	0.,	505.0,	528.0,	2.0,	2.0,	2., 3.
12,	218.2,	58.4,	0.12,	0.20					
		271.6,	0.12,	0.20,	85.6,	0.10,	0.20		
4.5,	4.5,	0.,	0.,	0.,	564.0,	589.0,	1.0,	2.0,	2., 2.
13,	256.7,	48.3,	0.19,	0.20					
		276.2,	0.19,	0.20,	66.6,	0.09,	0.25		
4.5,	4.5,	0.,	0.,	0.,	652.0,	3017.0,	2.0,	2.0,	2., 1.
14,	417.7,	29.7,	0.07,	0.22					
		1431.0,	0.07,	0.22,	27.8,	0.03,	0.25		
4.5,	4.5,	0.,	0.,	0.,	707.0,	3075.0,	1.0,	2.0,	2., 0.
15,	5.0,	2462.0,	0.75,	-0.20					
		2780.0,	0.75,	-0.20,	2884.4,	0.40,	-0.20		
4.5,	4.5,	0.,	0.,	0.,	3224.0,	3224.0,	2.0,	0.,	1., 1.
16,	4.7,	2618.9,	0.71,	-0.20					
		3008.0,	0.71,	-0.20,	2621.0,	0.01,	-0.20		
4.5,	4.5,	0.,	0.,	0.,	3493.0,	3493.0,	1.0,	0.,	1., 0.

1,	1048.2,	11.8,	0.25,	1.00					
4.0,	4.0,	0.62,	11.8,	0.25,	1.00,	11.6,	0.06,	1.00	
2,	4348.1,	19.5,	0.40,	0.40,	0.60,	15.8,	29.2,	6.0,	2.0, 3., 7.
		17.2,	0.47,	0.20,					
4.2,	4.4,	0.30,	0.20,	0.60,	0.60,	17.2,	0.18,	-0.20	
3,	878.7,	14.1,	0.58,	0.20,		27.6,	41.7,	5.0,	2.0, 3., 6.
		24.7,	0.58,	0.20,					
4.5,	4.5,	0.20,	0.	0.60,	0.	29.8,	0.49,	0.20	
4,	850.6,	14.6,	0.04,	0.20,		40.9,	55.5,	4.0,	2.0, 3., 5.
		35.6,	0.04,	0.20,					
4.5,	4.5,	0.	0.	0.	0.	35.6,	0.41,	0.20	
5,	558.0,	24.2,	0.23,	0.20,		59.7,	70.4,	3.0,	2.0, 3., 4.
		30.4,	0.23,	0.20,					
4.5,	4.5,	0.	0.	0.	0.	17.6,	0.06,	0.20	
6,	462.0,	27.1,	0.67,	0.20,		75.2,	87.6,	2.0,	2.0, 3., 3.
		40.7,	0.67,	0.20,					
4.5,	4.5,	0.	0.	0.	0.	22.6,	0.46,	0.20	
7,	585.8,	21.2,	0.86,	0.20,		91.2,	105.0,	1.0,	2.0, 3., 2.
		45.6,	0.86,	0.20,					
4.5,	4.5,	0.	0.	0.	0.	33.6,	0.32,	0.20	
8,	700.7,	17.7,	0.48,	0.20,		125.0,	373.0,	2.0,	6.0, 3., 1.
		67.1,	0.48,	0.20,					
4.5,	4.5,	0.	0.	0.	0.	41.2,	0.42,	0.20	
9,	48.7,	254.4,	0.18,	0.20,		143.0,	394.0,	1.0,	6.0, 3., 0.
		324.1,	0.18,	0.20,					
4.5,	4.5,	0.	0.	0.	0.	344.0,	0.10,	0.20	
10,	43.7,	283.5,	0.01,	-0.20,		423.0,	498.0,	6.0,	2.0, 2., 7.
		311.4,	0.01,	-0.20,					
4.5,	4.5,	0.	0.	0.	0.	288.5,	0.01,	-0.20	
11,	188.8,	68.1,	0.10,	0.20,		479.0,	545.0,	5.0,	2.0, 2., 6.
		219.6,	0.10,	0.20,					
4.5,	4.5,	0.	0.	0.	0.	90.5,	0.28,	0.20	
12,	154.4,	92.4,	0.19,	0.20,		539.0,	594.0,	4.0,	2.0, 2., 5.
		249.3,	0.19,	0.20,					
4.5,	4.5,	0.	0.	0.	0.	76.1,	0.10,	0.20	
13,	184.9,	77.6,	0.15,	0.20,		618.0,	644.0,	3.0,	2.0, 2., 4.
		308.5,	0.15,	0.20,					
4.5,	4.5,	0.	0.	0.	0.	86.6,	0.13,	0.20	
14,	187.9,	68.8,	0.12,	0.20,		686.0,	713.0,	2.0,	2.0, 2., 3.
		328.8,	0.12,	0.20,					
4.5,	4.5,	0.	0.	0.	0.	63.8,	0.07,	0.20	
15,	221.1,	56.1,	0.21,	0.20,		755.0,	784.0,	1.0,	2.0, 2., 2.
		278.6,	0.21,	0.20,					
4.5,	4.5,	0.	0.	0.	0.	76.3,	0.09,	0.20	
16,	353.9,	35.0,	0.06,	0.20,		855.0,	3885.0,	2.0,	2.0, 2., 1.
		335.0,	0.06,	0.20,					
4.5,	4.5,	0.	0.	0.	0.	1440.6,	0.03,	0.20	
17,	560.2,	22.2,	0.05,	0.20,		918.0,	3951.0,	1.0,	2.0, 2., 0.
		2577.0,	0.05,	0.20,					
4.5,	4.5,	0.	0.	0.	0.	3005.0,	0.	0.20	
18,	3.7,	3322.0,	0.01,	0.20,		4121.0,	4121.0,	2.0,	0., 1., 1.
		3801.0,	0.01,	0.20,					
4.5,	4.5,	0.	0.	0.	0.	3317.3,	0.01,	0.20	
						4426.0,	4426.0,	1.0,	0., 1., 0.

1,	0.	0.	1.20,	0.80					
			3.5,	1.20,	0.80,	0.	0.	0.	
4.0,	3.5,	0.40,	0.70,	0.60,	0.40,	6.8,	8.0,	2.0,	2.0, 4., 1.
2,	0.	0.	0.	1.00,	0.80				
			3.5,	1.00,	0.80,	0.	0.	0.	
4.4,	3.9,	0.	0.50,	0.	0.60,	13.6,	15.0,	1.0,	2.0, 3., 10.
3,	0.	0.	0.	0.24,	0.80				
			9.6,	0.24,	0.80,	0.	0.	0.	
4.5,	4.5,	0.30,	0.20,	0.60,	0.60,	27.7,	68.0,	2.0,	6.0, 3., 9.
4,	0.	0.	0.	3.40,	0.65				
			40.0,	3.40,	0.65,	16.0,	0.05,	-0.25	
4.5,	4.5,	0.	0.	0.	0.	43.2,	83.0,	1.0,	6.0, 3., 8.
5,	0.	0.	0.	5.30,	0.65				
			49.0,	5.30,	0.65,	0.	0.	0.	
4.5,	4.5,	0.	0.	0.	0.	99.9,	124.0,	6.0,	2.0, 3., 7.
6,	0.	0.	0.	0.20,	0.80				
			13.0,	0.20,	0.80,	50.0,	3.00,	0.65	
4.5,	4.5,	0.	0.	0.	0.	120.0,	144.0,	5.0,	2.0, 3., 6.
7,	0.	0.	0.	0.30,	0.77				
			25.0,	0.30,	0.77,	48.0,	2.20,	0.80	
4.5,	4.5,	0.	0.	0.	0.	141.0,	165.0,	4.0,	2.0, 3., 5.
8,	0.	0.	0.	0.50,	0.80				
			25.0,	0.50,	0.80,	46.1,	1.90,	0.80	
4.5,	4.5,	0.	0.	0.	0.	170.0,	188.0,	3.0,	2.0, 3., 4.
9,	0.	0.	0.	0.60,	0.80				
			25.0,	0.60,	0.80,	45.0,	1.00,	0.80	
4.5,	4.5,	0.	0.	0.	0.	193.0,	213.0,	2.0,	2.0, 3., 3.
10,	0.	0.	0.	0.10,	0.80				
			26.3,	0.10,	0.80,	42.8,	0.79,	0.80	
4.5,	4.5,	0.	0.	0.	0.	217.0,	238.0,	1.0,	2.0, 3., 2.
11,	386.1,		32.1,	0.96,	0.80				
			32.1,	0.96,	0.80,	140.0,	1.20,	-0.25	
4.5,	4.5,	0.	0.	0.	0.	266.0,	723.0,	2.0,	6.0, 3., 1.
12,	460.7,		26.9,	0.48,	0.80				
			26.5,	0.48,	0.80,	151.0,	0.90,	-0.25	
4.5,	4.5,	0.	0.	0.	0.	292.0,	753.0,	1.0,	6.0, 3., 0.
13,	19.2,		645.0,	2.90,	-0.25				
			525.0,	2.90,	-0.25,	642.0,	1.00,	-0.25	
4.5,	4.5,	0.	0.	0.	0.	789.0,	891.0,	6.0,	2.0, 2., 7.
14,	0.	0.	0.	0.05,	0.80				
			88.0,	0.05,	0.80,	520.0,	8.00,	-0.25	
4.5,	4.5,	0.	0.	0.	0.	863.0,	951.0,	5.0,	2.0, 2., 6.
15,	140.4,		88.3,	0.10,	0.80				
			88.0,	0.10,	0.80,	610.0,	1.60,	-0.25	
4.5,	4.5,	0.	0.	0.	0.	942.0,	1015.0,	4.0,	2.0, 2., 5.
16,	0.	0.	0.	0.11,	0.80				
			75.0,	0.11,	0.80,	645.0,	1.60,	-0.25	
4.5,	4.5,	0.	0.	0.	0.	1044.0,	1077.0,	3.0,	2.0, 2., 4.
17,	142.0,		87.2,	0.16,	0.80				
			70.0,	0.16,	0.80,	680.0,	1.20,	-0.25	
4.5,	4.5,	0.	0.	0.	0.	1131.0,	1165.0,	2.0,	2.0, 2., 3.
18,	197.8,		62.6,	0.16,	0.80				
			81.0,	0.16,	0.80,	800.0,	0.75,	-0.25	
4.5,	4.5,	0.	0.	0.	0.	1221.0,	1256.0,	1.0,	2.0, 2., 2.
19,	169.3,		73.2,	0.18,	0.80				
			73.2,	0.18,	0.80,	816.0,	2.25,	-0.25	
4.5,	4.5,	0.	0.	0.	0.	1346.0,	5959.0,	2.0,	2.0, 2., 1.
20,	259.2,		47.8,	0.07,	0.80				
			48.0,	0.07,	0.80,	814.0,	1.10,	-0.25	
4.5,	4.5,	0.	0.	0.	0.	1425.0,	6041.0,	1.0,	2.0, 2., 0.
21,	2.6,		4729.0,	0.80,	-1.00				
			4730.0,	0.80,	-1.00,	5560.0,	0.16,	-0.25	
4.5,	4.5,	0.	0.	0.	0.	6249.0,	6249.0,	2.0,	0., 1., 1.
22,	2.2,		4936.0,	0.42,	-0.50				
			4970.0,	0.42,	-0.50,	5890.0,	0.08,	-0.25	
4.5,	4.5,	0.	0.	0.	0.	6626.0,	6626.0,	1.0,	0., 1., 0.

1,	0.	0.	0.	0.	0.	28.0	0.	0.	0.	0.	0.
4.0,	2.7,	0.	0.90,	0.	0.20,	6.8,	8.2,	1.0,	5.0,	4.,	13.
2,	0.		10.0,	1.80,	0.75						
			10.0,	1.80,	0.75,	7.0,	0.25,	0.75			
3.4,	4.4,	0.80,	0.30,	0.50,	0.60,	16.5,	67.0,	5.0,	6.0,	3.,	12.
3,	0.		15.0,	2.00,	0.75						
			15.0,	2.00,	0.75,	15.0,	0.25,	0.75			
4.2,	4.5,	0.50,	0.60,	0.60,	0.60,	31.0,	86.0,	4.0,	6.0,	3.,	11.
4,	0.		20.0,	2.30,	0.75						
			20.0,	2.30,	0.75,	20.0,	0.31,	0.75			
4.5,	4.5,	0.20,	0.	0.60,	0.	49.1,	104.0,	3.0,	6.0,	3.,	10.
5,	0.		20.0,	2.45,	0.81						
			20.0,	2.45,	0.81,	30.0,	0.31,	0.78			
4.5,	4.5,	0.	0.	0.	0.	69.4,	123.0,	2.0,	6.0,	3.,	9.
6,	336.2,		40.0,	2.60,	0.80						
			40.0,	2.60,	0.80,	50.0,	0.26,	0.78			
4.5,	4.5,	0.	0.	0.	0.	90.0,	142.0,	1.0,	6.0,	3.,	8.
7,	202.8,		62.0,	4.00,	0.79						
			62.0,	4.00,	0.79,	110.0,	0.15,	0.71			
4.5,	4.5,	0.	0.	0.	0.	160.0,	191.0,	6.0,	2.0,	3.,	7.
8,	205.0,		60.0,	3.00,	0.81						
			60.0,	3.00,	0.81,	30.0,	0.18,	0.90			
4.5,	4.5,	0.	0.	0.	0.	184.0,	214.0,	5.0,	2.0,	3.,	6.
9,	0.		58.0,	2.30,	0.82						
			58.0,	2.30,	0.82,	30.0,	0.33,	0.94			
4.5,	4.5,	0.	0.	0.	0.	209.0,	238.0,	4.0,	2.0,	3.,	5.
10,	0.		56.0,	2.10,	0.85						
			56.0,	2.10,	0.85,	30.0,	0.50,	0.95			
4.5,	4.5,	0.	0.	0.	0.	244.0,	266.0,	3.0,	2.0,	3.,	4.
11,	0.		52.0,	0.90,	0.88						
			52.0,	0.90,	0.88,	34.0,	0.65,	0.95			
4.5,	4.5,	0.	0.	0.	0.	270.0,	294.0,	2.0,	2.0,	3.,	3.
12,	0.		50.0,	0.38,	0.95						
			50.0,	0.38,	0.95,	32.0,	0.77,	1.18			
4.5,	4.5,	0.	0.	0.	0.	298.0,	323.0,	1.0,	2.0,	3.,	2.
13,	328.3,		37.0,	0.90,	0.19						
			37.0,	0.90,	0.19,	185.0,	0.36,	0.78			
4.5,	4.5,	0.	0.	0.	0.	354.0,	940.0,	2.0,	6.0,	3.,	1.
14,	389.8,		31.0,	0.45,	1.28						
			31.0,	0.45,	1.28,	200.0,	0.21,	0.81			
4.5,	4.5,	0.	0.	0.	0.	384.0,	974.0,	1.0,	6.0,	3.,	0.
15,	0.		650.0,	2.20,	0.73						
			650.0,	2.20,	0.73,	0.	0.	0.			
4.5,	4.5,	0.	0.	0.	0.	1010.6,	1129.0,	6.0,	2.0,	2.,	7.
16,	106.6,		110.0,	0.06,	1.02						
			110.0,	0.06,	1.02,	700.0,	4.60,	0.75			
4.5,	4.5,	0.	0.	0.	0.	1097.0,	1197.0,	5.0,	2.0,	2.,	6.
17,	122.9,		100.0,	0.11,	1.05						
			100.0,	0.11,	1.05,	775.0,	1.60,	0.75			
4.5,	4.5,	0.	0.	0.	0.	1185.0,	1267.0,	4.0,	2.0,	2.,	5.
18,	149.8,		85.0,	0.13,	1.14						
			85.0,	0.13,	1.14,	800.0,	1.60,	0.75			
4.5,	4.5,	0.	0.	0.	0.	1299.0,	1336.0,	3.0,	2.0,	2.,	4.
19,	138.4,		90.0,	0.16,	1.15						
			90.0,	0.16,	1.15,	850.0,	1.20,	0.77			
4.5,	4.5,	0.	0.	0.	0.	1396.0,	1434.0,	2.0,	2.0,	2.,	3.
20,	0.		85.0,	0.16,	1.20						
			85.0,	0.16,	1.20,	875.0,	0.65,	0.88			
4.5,	4.5,	0.	0.	0.	0.	1496.0,	1535.0,	1.0,	2.0,	2.,	2.
21,	149.9,		83.0,	0.17,	1.20						
			83.0,	0.17,	1.20,	950.0,	0.63,	0.78			
4.5,	4.5,	0.	0.	0.	0.	1634.0,	7164.0,	2.0,	2.0,	2.,	1.
22,	223.0,		50.0,	0.07,	1.50						
			50.0,	0.07,	1.50,	990.0,	0.37,	0.88			
4.5,	4.5,	0.	0.	0.	0.	1721.4,	7254.0,	1.0,	2.0,	2.,	0.
23,	2.2,		5700.0,	0.78,	0.80						
			5700.0,	0.78,	0.80,	0.	0.	0.			
4.5,	0.	0.	0.	0.	0.	7482.0,	7482.0,	2.0,	0.	1.,	1.
24,	2.1,		5900.0,	0.42,	0.85						

		108.0	0.21	0.80	1200.0	1.00	-0.25					
4.5	4.5	0.	0.	0.	2131.0	2178.0	1.0	2.0	2.	2.		
25	118.0	107.0	0.15	0.80								
		105.0	0.15	0.80	1327.0	0.87	-0.25					
4.5	4.5	0.	0.	0.	2295.0	9914.0	2.0	2.0	2.	2.	1.	
26	165.0	75.0	0.07	0.80								
		67.7	0.07	0.80	1367.0	0.56	-0.25					
4.5	4.5	0.	0.	0.	2399.0	10020.0	1.0	2.0	2.	2.	0.	
27	1.0	7800.0	0.77	-0.80								
		7804.0	0.77	-0.80	9170.0	0.24	-0.25					
4.5	4.5	0.	0.	0.	10290.0	10288.0	2.0	0.	1.	1.	1.	
28	0.	8000.0	0.42	-0.42								
		8049.0	0.42	-0.42	9578.0	0.15	-0.35					
4.5	4.5	0.	0.	0.	10775.0	10775.0	1.0	0.	1.	1.	0.	

			122.0,	0.16,	0.80,	1227.0,	1.40,	-0.25		
4.5,	4.5,	0.	, 0.	, 0.	, 0.	, 2182.0,	2229.0,	2.0,	2.0,	2., 3.
25,	98.9,		125.4,	0.21,	0.80					
			118.0,	0.21,	0.80,	1300.0,	1.00,	-0.25		
4.5,	4.5,	0.	, 0.	, 0.	, 0.	, 2308.0,	2357.0,	1.0,	2.0,	2., 2.
26,	111.0,		111.6,	0.15,	0.80					
			100.0,	0.15,	0.80,	1427.0,	0.87,	-0.25		
4.5,	4.5,	0.	, 0.	, 0.	, 0.	, 2478.0,	10672.0,	2.0,	2.0,	2., 1.
27,	192.0,		64.6,	0.07,	0.80					
			68.0,	0.07,	0.80,	1567.0,	0.56,	-0.25		
4.5,	4.5,	0.	, 0.	, 0.	, 0.	, 2585.0,	11062.0,	1.0,	2.0,	2., 0.
28,	1.5,		8322.0,	0.77,	-0.80					
			8322.0,	0.77,	-0.80,	9763.0,	0.24,	-0.25		
4.5,	4.5,	0.	, 0.	, 0.	, 0.	, 11062.0,	11062.0,	2.0,	0.	, 1., 1.
29,	1.4,		8611.0,	0.42,	-0.42					
			8611.0,	0.42,	-0.42,	9578.0,	0.15,	-0.35		
4.5,	4.5,	0.	, 0.	, 0.	, 0.	, 11566.0,	11566.0,	1.0,	0.	, 1., 0.